Part IV

Intercomparison and Interpretation of Results

Scientific Results from the EPOCH'92 Observations Organized by the USNO

T.M. Eubanks, B.A. Archinal, M.S. Carter, F.J. Josties, K.A. Kingham, J.O. Martin, D.N. Matsakis and D.D. McCarthy

U.S. Naval Observatory, Washington, D.C., 20392

ABSTRACT. In order to assess the reality of any high frequency rotational variations observed during the EPOCH'92 campaign, a series of special Navy-Experimental Global (or NAVEX-G) sessions were coordinated by the USNO to provide periods of observations by two independent Very Long Baseline Interferometry (VLBI) networks during part of EPOCH'92. The NAVEX-G network used the NAVNET Green Bank antenna together with radio telescopes in Chile, Italy, South Africa, Canada and Japan. This truly global network provided orientation accuracy comparable to the lower noise (but smaller) NASA network run simultaneously, and thus a means of assessing the validity of any small high frequency variations in Earth orientation observed during this period. This paper presents a brief description of these NAVEX-G observations and the results obtained from them.

1. INTRODUCTION

The SEARCH-92 campaign organized by the International Earth Rotation Service included a special observing period called EPOCH'92 (July 25-August 8, 1992), intended to study high-frequency variations in Earth rotation. To complement the period of almost continuous VLBI observations organized by the U.S. National Aeronautics and Space Administration (NASA), the U.S. Naval Observatory (USNO), in addition to the on-going weekly NAVNET VLBI sessions, organized a series of four Navy Experimental-Global (NAVEX-G) observing sessions using VLBI antennas in Green Bank, (U.S.A.), Algonquin (Canada), Kashima (Japan), Matera (Italy), Santiago (Chile) and Hartebeesthoek (South Africa). The primary purpose of these NAVEX-G observations was to determine the reality of high frequency variations in the orientation of the Earth, and the level of systematic and random errors in VLBI determinations of these variations, through comparisons between independent simultaneous VLBI sessions of the highest possible quality. The NAVEX-G observations were fully successful in meeting these goals, and high quality data were obtained from each session, with a total of 2247 successful observations being obtained (in addition to the 1293 observations obtained from regular NAVNET sessions during EPOCH'92).

2. RESULTS OF THE NAVEX-G EPOCH'92 OBSERVATIONS

The NAVEX-G measurements sessions were intended to, and did, provide Earth orientation estimation accuracy comparable to the simultaneous NASA Research and Development (R&D) sessions. The NAVEX-G achieved this accuracy through the use of a truly global network with up to 6 stations in 5 continents, the size of the network being specifically intended to compensate for the sensitivity of the R&D observations. Data were obtained on baselines up to 12,419 km long, and the bulk of the data were obtained from baselines of about 1 1/2 Earth radii in length. Good results were obtained from these long baselines, and the actual UT1 and polar motion formal errors from the two networks were roughly equal. Both networks provided roughly a factor of two increase in sensitivity over that obtained by the IRIS-A and NAVNET sessions during the same period.

The existing IERS standards [1] were found to be inadequate to reduce the global scale NAVEX-G sessions due to their neglect of the tidally driven diurnal and semidiurnal variations in UT1 and polar motion. This effect is striking in the NAVEX-G sessions during EPOCH'92. When these data are reduced in the standard fashion, estimating one set of 24 hour averaged values for UT1, polar motion and nutation offsets, the weighted root mean square (rms) post-fit residual scatter of the interferometric delays was

±52.0 picoseconds. When the data are used to estimate hourly piecewise linear variations in UT1 and polar motion, the weighted rms drops to ±43.6 picoseconds (a strongly significant 30% reduction in variance). The data processing for future global NAVEX sessions was modified to do a final editing and weighting of the data using the hourly piecewise linear parametrization of high-frequency Earth orientation changes.

The NAVEX-G data have been used in a number of initial comparisons between simultaneous VLBI sessions ([2], [3]), as well as in comparisons between VLBI and data from the Global Positioning system (see, e.g., [4]), and with other data types such as atmospheric angular momentum data. When the EPOCH'92 R&D and NAVEX-G VLBI data are used to estimate the UT1 and polar motion on an hourly basis, there are 104 hourly values with simultaneous data. The R&D and NAVEX-G data have an rms difference (in all three components of Earth orientation) of about ±0.5 milli arc seconds (mas). Although in polar motion the observed residual scatter is consistent with the root sum square (rss) of the R&D and NAVEX-G formal errors, the UT1 differences are significantly larger than would be expected from the formal errors, evidence of roughly ±0.4 mas of unmodeled errors. In general, the observed hourly fluctuations in UT1 and polar motion agree well, but not perfectly, with independent models of the tidally forced diurnal and semi-diurnal orientation changes, and it is clear that these tidal variations are the dominant source of orientation changes at periods between about two days and one hour. These comparisons bound any non-tidal variations in orientation in this period range during EPOCH'92 to be ≤ about 0.4 mas rms in all three components of orientation

The EPOCH'92 results show that accurate, high quality VLBI Earth orientation results can be obtained from global networks. Global scale VLBI offers a number of advantages, including the maximum sensitivity to Earth orientation changes and the best means of decoupling orientation changes from local and regional motions of the antennas, such as those caused by ocean tidal loading. Global scale VLBI also avoids the "edge effect" found in smaller networks, where certain stations on the edge of the network cannot obtain complete sky coverage due to their distance from the rest of the network. In order to investigate the long term stability and accuracy of orientation results from global networks the USNO organized a series of six global sessions during 1993, with the number of stations used being increased from six to a maximum of ten. These large networks thus have sufficient redundancy to be divided into sub-networks, each providing independent orientation data of good quality. This on-going work thus extends and complements the EPOCH'92 NAVEX-G simultaneous sessions, in order to determine better the sources of systematic error limiting the accuracy of geodetic VLBI. Similar global experiments were organized during the January, 1994, CONT-94 period, to provide another period of simultaneous observations between independent VLBI networks.

ACKNOWLEDGEMENTS. These results represent a truly international effort, and would not have been possible without contributions from (among others) the Agenzia Spaziale Italiana, the Hartebeesthoek Radio Astronomy Observatory, the Communications Research Laboratory in Japan, the Institut fur Angewandte Geodasie in Germany, the National Radio Astronomy Observatory and the NASA/Goddard VLBI group.

REFERENCES

1. McCarthy, D.D., (edt.), IERS Standards (1992), International Earth Rotation Service Technical Note Number 13, Observatoire de Paris, Paris (1992).
2. Eubanks, T.M., B.A. Archinal, M.S. Carter, F.J. Josties, K.A. Kingham, J.O. Martin, D.N. Matsakis and D.D. McCarthy, The Contribution to the EPOCH'92 Measurement Campaign Organized by the U.S. Naval Observatory, EOS Trans. AGU, 73, 135, (1992).
3. Ma, C., T.A. Clark, J.W. Ryan, J.M. Gipson, D.S. MacMillian, C.C. Thomas, N.R. Vandenberg, D. Gordon and A.E. Niell, VLBI EOP Observations during the EPOCH'92 Campaign, EOS Trans. AGU, 74, 105, (1993).
4. Freedman, A.P., R. Ibanez-Meier, J.O. Dickey, S.M. Lichten and T.A. Herring, Sub-Daily Earth Rotation during the Epoch'92 Campaign, pp. 202-211 in the Proceedings of the 1993 IGS Workshop, Beutler and Brockmann, edt., Druckerei der Universitat Bern (1993).

KALMAN FILTER ANALYSIS OF SEARCH 92 VLBI DATA

T. A. HERRING
Massachusetts Institute of Technology,
77 Massachusetts Avenue,
Cambridge, MA 02139
USA

ABSTRACT: An analysis of the very long baseline interferometer data collected during the Epoch 1992 campaign is presented. A standard analysis is discussed in which tidally coherent, diurnal and semidiurnal polar motion and UT1-UTC variations are applied prior to Kalman filtering the VLBI data for stochastic estimates of 3-hourly binned estimated of pole position and UT1-UTC. Variants of this analysis are discussed to show the sensitivity of the results choice of process noise parameters and the apriori application of the tidally coherent models. Here the residuals between a smoothed VLBI polar motion and UT1 apriori series are shown. For pole position, this apriori series is very similar to IERS Bulletin B. For UT1, the use of the VLBI series reduces by half the size of the UT1 residuals compared to IERS Bulletin B.

1. Introduction

We present here the analysis of the SEARCH 92 VLBI data set using two different analysis techniques: (1) estimation of sub-daily variations in polar motion and UT1 using a batched Kalman filter technique; and (2) direct estimation of the cosine and sine components of diurnal (frequency 1-cycle-per-sidereal day) and semidiurnal (2-cycles-per-sidereal day) signals in polar motion and UT1. The experiments analyzed here are listed in Table 1 along with the station participating in each experiment.

2. Data Analysis

The VLBI data were analyzed using the techniques discussed in Herring and Dong [1994]. The coordinates of the radio telescopes were constrained at the values determined from the analysis of VLBI data obtained between 1990 and 1993, and apriori constraint was taken to be the standard deviations obtained from the coordinate solution. The radio source positions were held fixed at the values obtained from 1990-1993 analysis. The MTT hydrostatic and wet functions used in the analysis [Herring, 1992] and the process noise used to stochastically model the wet delay variations was obtained using the algorithm discussed in Herring et al. [1990]. The ZMOA-1990-2 nutation series given in Herring [1991] was used as the apriori nutation series. Daily estimates of correction to this series were made in all analyses. The hydrogen masers were model with Allan standards of 10^{-14} at sampling intervals of 30 minutes as discussed in Herring et al. [1990].

TABLE 1: VLBI experiments analyzed

Start date	Description	Sites (first four characters)					
92/07/26	EUR9-HOFN-4	HOFN	WEST	GILC	WETT	ONSA	
92/07/27	IRISA-751	HOFN	WEST	GILC	WETT	ONSA	
92/07/28	Navex-G3	SANT	NRAO	KASH	HART	MATE	
92/07/28	RD-E-92A	WEST	FD-V	LA-V	GILC	KAUA	WETT
92/07/29	Navex-G4	SANT	ALGO	NRAO	KASH	HART	MATE
92/07/29	RDE-92B	WEST	FD-V	LA-V	GILC	KAUA	WETT
92/07/30	Navnet 187	RICH	MOJA	GILC	KAUA		
92/07/31	RDE-92C	WEST	FD-V	LA-V	GILC	KAUA	WETT
92/08/02	RDE-92D	WEST	LA-V	GILC	KAUA	WETT	
92/08/03	IRISA-752	WEST	ALGO	RICH	MOJA	WETT	
92/08/04	Navex-G5	SANT	NRAO	KASH	HART	MATE	
92/08/04	RDE-92E	WEST	FD-V	LA-V	GILC	KAUA	WETT
92/08/05	Navex-G6	SANT	ALGO	NRAO	KASH	HART	MATE
92/08/05	RDE-92	WEST	FD-V	LA-V	GILC	KAUA	WETT
92/08/06	Navnet-188	NRAO	RICH	MOJA	GILC	KAUA	
92/08/07	RDE-92G	WEST	FD-V	LA-V	GILC	KAUA	WETT
92/08/09	RDE-92H	WEST	FD-V	LA-V	GILC	KAUA	WETT
92/08/10	IRISA-753	WEST	ALGO	RICH	MOJA	WETT	
92/08/10	Navex-25	NRAO	GILC	KAUA	KASH	MATE	
92/08/11	XASIA-2	DSS45	HOBA	KASH	SESH	HART	WETT

The treatment of polar motion and UT1 subdaily variations differed between analyses. In our standard analysis, estimates of pole position and UT1 were make from batches of data approximately of 3 hours duration. The estimated values of the pole position and UT1 for each batch of data are reported at the epoch of the VLBI observation closest to the mid-point time of the batch. Constraints of 0.3 mas and 0.04 mts were placed on the changes between adjacent values of the adjustments to the apriori polar motion and UT1 values. Apriori corrections were made for the tidal coherent variations in pole position and UT1 based on the coefficients given in Herring and Dong [1994]. Residuals to the apriori polar motion and UT1 from this analysis are shown in Figures 1, 2 and 3. As has been shown in numerous pervious studies, the subdaily variations in polar motion and UT1 are dominated by diurnal and semidiurnal variations. Also shown in the Figures 1, 2 and 3 (offset from previous values) are the time variations in the rotation parameters computed from estimates of the cosine and sine terms with periods of exactly 1- and 2-cycles per sidereal day. The estimates of the coefficients used to generate these temporal variations are given in Tables 2 and 3 with the cosine and sine terms defined in Herring and Dong [1994]. For comparison, and offset from the previous values, we show the lower parts of Figures 1, 2 and 3, the temporal variations expected from the tidally coherent model given in Herring and Dong [1994].

To evaluate the sensitivity of our standard stochastic analysis to applying apriori the tidally coherent model to analysis, we repeated the standard analysis with the tidally coherent model removed. The results of this analysis along with the differences between it and the standard analysis are shown in Figures 4, 5 and 6. Visually the types of analysis look very similar although at individual times the differences can be large as 0.9 mas and 0.05 mts. The larger excursions are for points with large uncertainties and most likely result form the filter not being able to track the rapid variations that occur in the diurnal and semidiurnal variations. The root-mean-square (RMS) scatters of the differences between the two analysis are 0.18 mas, 0.14 mas and 0.05 mts for the X and Y pole positions and UT1, respectively. The RMS differences are between 15 and 34% of the standard deviations of the stochastic estimates of the pole position and UT1.

Table 2. Estimates of the cosine and sine components of diurnal and semidiurnal UT1 variations. The time refers to the time of the midpoint of each 24-hour session of VLBI data.

Date	Hr:min	Diurnal				Semidiurnal			
		cos (ms)	± (ms)	sin (ms)	± (ms)	cos (ms)	± (ms)	sin (ms)	± (ms)
7/26	17:58	-0.039	0.013	0.068	0.013	0.004	0.010	0.007	0.008
7/27	20:02	-0.015	0.017	0.021	0.015	0.010	0.012	0.019	0.009
7/28	21:01	-0.053	0.011	0.037	0.007	-0.007	0.007	0.020	0.008
7/28	23:02	-0.032	0.006	0.024	0.004	-0.026	0.004	0.021	0.004
7/30	03:01	-0.048	0.006	0.018	0.006	-0.030	0.005	0.015	0.005
7/30	03:01	-0.040	0.004	-0.008	0.006	-0.032	0.004	-0.003	0.004
7/31	05:59	-0.018	0.032	-0.036	0.038	-0.038	0.024	-0.045	0.022
8/01	09:59	-0.015	0.005	-0.023	0.004	-0.021	0.004	-0.014	0.004
8/02	16:02	0.000	0.004	-0.008	0.005	-0.024	0.005	-0.021	0.004
8/03	20:03	0.037	0.031	0.028	0.017	-0.024	0.015	-0.036	0.015
8/04	21:06	-0.005	0.011	0.033	0.007	0.024	0.007	-0.006	0.009
8/04	23:01	-0.008	0.007	0.041	0.006	0.007	0.006	-0.021	0.005
8/06	03:11	-0.005	0.007	0.033	0.007	0.001	0.006	-0.003	0.007
8/06	03:01	-0.005	0.005	0.043	0.008	-0.009	0.005	0.001	0.005
8/07	06:04	0.005	0.029	0.067	0.030	-0.029	0.020	-0.018	0.018
8/08	10:00	-0.016	0.004	0.036	0.004	0.010	0.004	0.005	0.003
8/09	16:01	-0.004	0.004	0.019	0.004	-0.003	0.004	0.007	0.003
8/10	19:59	-0.035	0.025	0.049	0.014	-0.006	0.012	0.025	0.013
8/11	04:32	-0.020	0.005	-0.003	0.009	-0.016	0.005	0.020	0.007
8/12	03:56	0.036	0.013	-0.054	0.024	-0.007	0.013	0.017	0.014

3. Discussion

In general, the continuity between adjacent VLBI experiments is very good in this analysis although in the figures this agreement can be deceptive because of the large diurnal and semidiurnal signals present in the result. Differences between adjacent days and for the overlapping experiments are less than 0.5 mas for pole position and 0.08 ms for UT1-AT. The largest difference between simultaneous experiments if for the experiments that start on

July 28. While this difference may be related to the coordinates of the stations being in slightly different reference frames, this explanation seem unlikely because the networks used in the simultaneous experiments starting on July 29 are almost identical. (Algonquin Observatory was added to the USNO experiment on July 29, Also the discontinuity from the previous day is for the R&D experiment which used the same network on July 29.). We have investigated the possible effects of azimuthal asymmetry in the atmosphere using the model discussed in Rogers et al. [1993] but estimation of such parameters only slightly reduced (to 0.07 ms) the difference in UT1-AT for the experiments starting July, 28. The gradients estimated at Westford were the largest during this R&D experiment (magnitude corresponding to 80 mm delay at 5° elevation angle) and may indicate that the difference is atmospheric delay related but that the parameterization used in our analysis is not adequate to represent the phenomena.

The other aspect of this data set is the differences between the precision of different VLBI networks to measure high frequency Earth rotation changes. Most of these differences seem related to size and shape of the VLBI networks themselves. The variations in the standard deviations of the diurnal and semidiurnal signals given in Tables 2 and 3 show the amount variation in the current networks. From these tables, there is almost a factor of ten between the smallest and largest deviations of the estimates of these signals.

References

Herring, T. A., J. L. Davis, and I. I. Shapiro, (1990) Geodesy by radio interferometry: The application of Kalman filtering to the analysis of VLBI data, *J. Geophys. Res.*, *95*, 12561–12581.

Herring, T. A., (1991) The ZMOA-1990 nutation series, in *Proceedings of IAU colloquium No. 127, Reference Systems*, 157–166, US Naval Observatory,, Washington. D.C..

Herring, T. A., Modeling (1992) Atmospheric Delays in the Analysis of Space Geodetic Data, in *Proceeding of Refraction of Transatmospheric Signals in Geodesy*, edited by J. C. D. a. T. A. Th.Spoelstra, pp. 157–164, Netherlands Geodetic Commission, Publications on Geodesy, The Hague, Netherlands.

Herring, T. A., and D. Dong (1994) Measurement of Diurnal and Semidiurnal rotational variations and tidal parameters of the Earth, *J. Geophs. Res.*, in press.

Rogers et al., (1993) Improvements in the accuracy of geodetic VLBI, in Contributions of Space Geodesy to Geodynamics: Technology, eds. D. E. Smith and D. L. Turcotte, AGU Geodynamics Series Vol 25, pp. 47–64.

Table 3. Estimates of the cosine and sine components of diurnal and semidiurnal polar motion variations. The time refers to the time of the midpoint of each 24-hour session of VLBI data.

Date	Hr:min	Retrograde Semidiurnal				Prograde Semidiurnal			
		cos (mas)	± (mas)	sin (mas)	± (mas)	cos (mas)	± (mas)	sin (mas)	± (mas)
7/26	17:58	-0.282	0.201	-0.142	0.215	-0.048	0.213	0.448	0.216
7/27	20:02	0.070	0.249	0.013	0.233	0.521	0.246	0.370	0.253
7/28	21:01	0.270	0.081	-0.076	0.077	0.011	0.085	0.200	0.075
7/28	23:02	0.366	0.088	-0.412	0.091	0.014	0.083	0.036	0.092
7/30	03:01	0.464	0.061	0.108	0.059	0.231	0.064	-0.083	0.055
7/30	03:01	0.435	0.075	-0.241	0.079	0.040	0.077	0.088	0.078
7/31	05:59	0.276	0.332	-0.246	0.276	-0.348	0.271	0.557	0.306
8/01	09:59	0.432	0.069	0.468	0.073	0.086	0.065	-0.080	0.073
8/02	16:02	0.083	0.080	0.478	0.079	-0.108	0.077	0.129	0.081
8/03	20:03	-0.510	0.218	0.261	0.208	-0.202	0.214	0.496	0.223
8/04	21:06	-0.050	0.102	0.116	0.103	-0.026	0.104	-0.012	0.101
8/04	23:01	0.261	0.091	0.411	0.092	0.152	0.089	0.221	0.096
8/06	03:11	-0.040	0.073	0.059	0.067	-0.075	0.071	-0.249	0.065
8/06	03:01	-0.362	0.078	0.253	0.078	-0.080	0.077	0.040	0.082
8/07	06:04	-0.194	0.228	0.101	0.202	-0.001	0.207	0.119	0.216
8/08	10:00	0.083	0.068	-0.067	0.063	0.093	0.062	0.147	0.070
8/09	16:01	0.206	0.075	-0.267	0.070	0.041	0.070	0.002	0.075
8/10	19:59	0.149	0.179	0.049	0.173	-0.130	0.175	0.000	0.195
8/11	04:32	0.163	0.114	0.034	0.120	0.157	0.108	0.092	0.121
8/12	03:56	0.145	0.087	0.154	0.081	0.034	0.084	-0.054	0.080

Date	Hr:min	Prograde diurnal			
		cos (mas)	± (mas)	sin (mas)	± (mas)
7/26	17:58	-0.841	0.290	0.038	0.329
7/27	20:02	-0.037	0.332	-0.229	0.358
7/28	21:01	0.036	0.092	0.316	0.092
7/28	23:02	-0.260	0.103	0.359	0.115
7/30	03:01	0.016	0.060	0.429	0.065
7/30	03:01	0.136	0.106	0.253	0.099
7/31	05:59	0.312	0.406	0.248	0.442
8/01	09:59	0.106	0.085	0.219	0.072
8/02	16:02	-0.145	0.090	0.063	0.092
8/03	20:03	-0.188	0.314	0.410	0.340
8/04	21:06	-0.198	0.132	0.001	0.146
8/04	23:01	-0.168	0.124	-0.392	0.101
8/06	03:11	-0.279	0.074	-0.041	0.075
8/06	03:01	-0.244	0.107	-0.128	0.103
8/07	06:04	-0.691	0.289	0.049	0.313
8/08	10:00	-0.365	0.076	-0.010	0.072
8/09	16:01	-0.133	0.087	-0.026	0.083
8/10	19:59	-0.247	0.267	-0.427	0.297
8/11	04:32	-0.241	0.137	0.173	0.168
8/12	03:56	-0.216	0.130	0.335	0.100

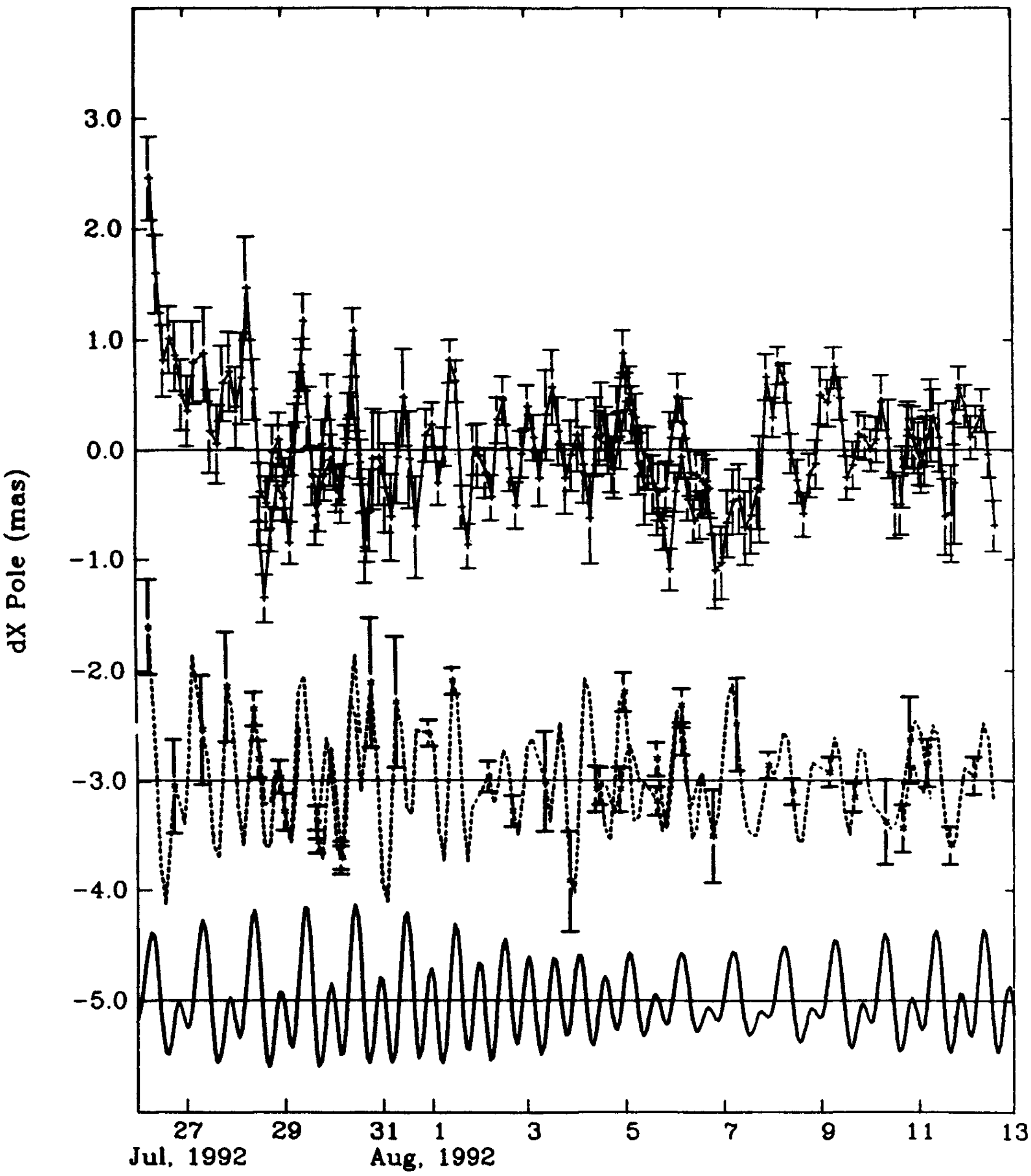

Figure 1. Differences between the stochastic estimates of the X-pole position for the standard analysis discussed in the text (top part of figure). The middle portion of the figure shows with a dashed line the time-domain representation of the diurnal and semidiurnal coefficient estimates (Table 2). Occasional one-standard deviation error bars are shown computed from the standard deviations of the coefficient estimates. The lower part of the figure shows the time domain representation of the tidally coherent signals given in Herring and Dong [1994]

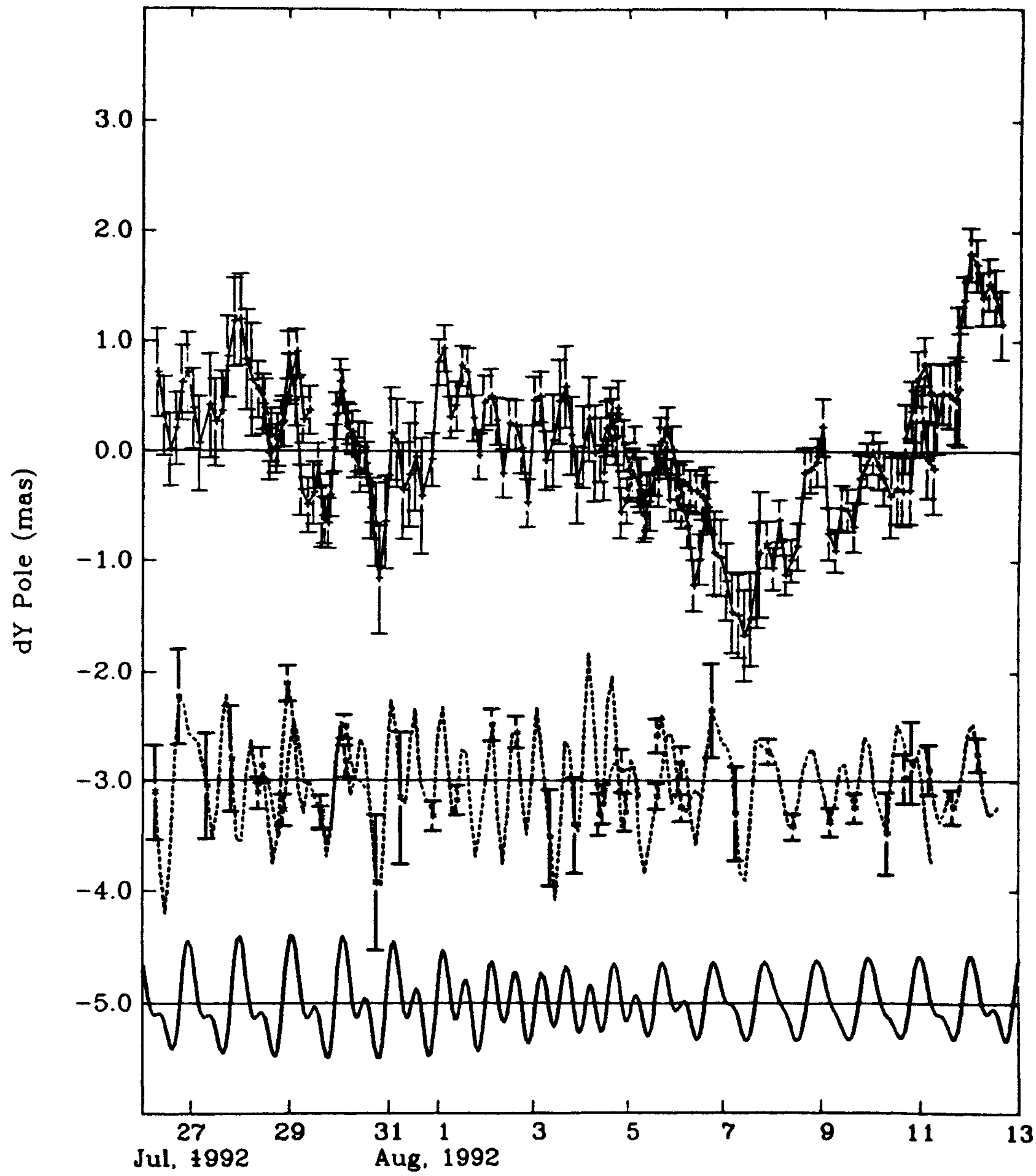

Figure 2. Same as Figure 1 except Y-pole position differences are shown.

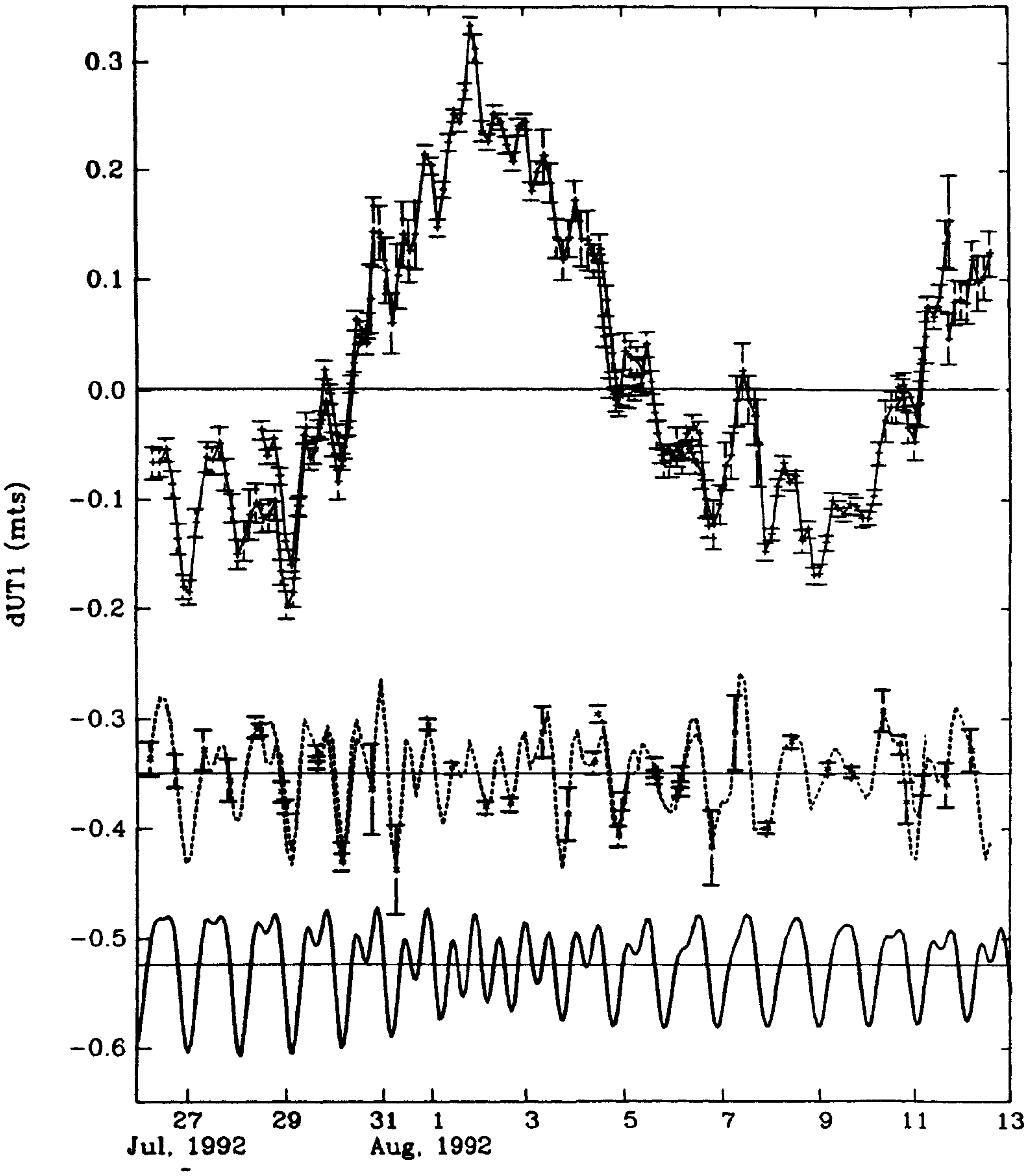

Figure 3. Same as Figure 1 except UT1-AT differences are shown.

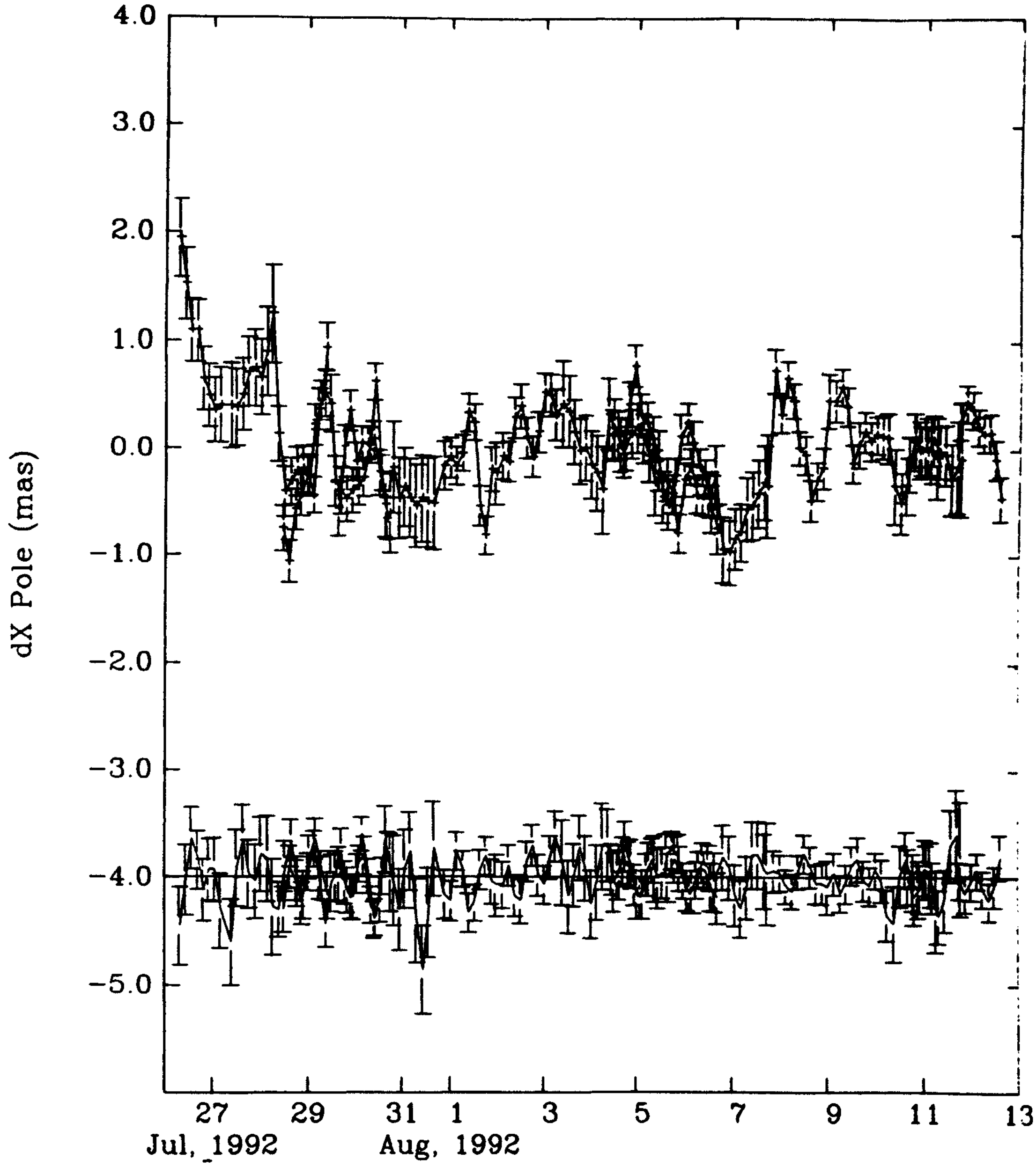

Figure 4. Differences between the stochastic estimates of the X-pole position for the standard analysis discussed in the text except that no diurnal and semidiurnal polar motion and UT1 variations were applied apriori (top portion of figure). The lower portion the differences between the standard analysis and this analysis are shown. Most of the differences can be explained by the stochastics not being able to track the rapid variations in the diurnal and semidiurnal signals when the VLBI data geometry is weak.

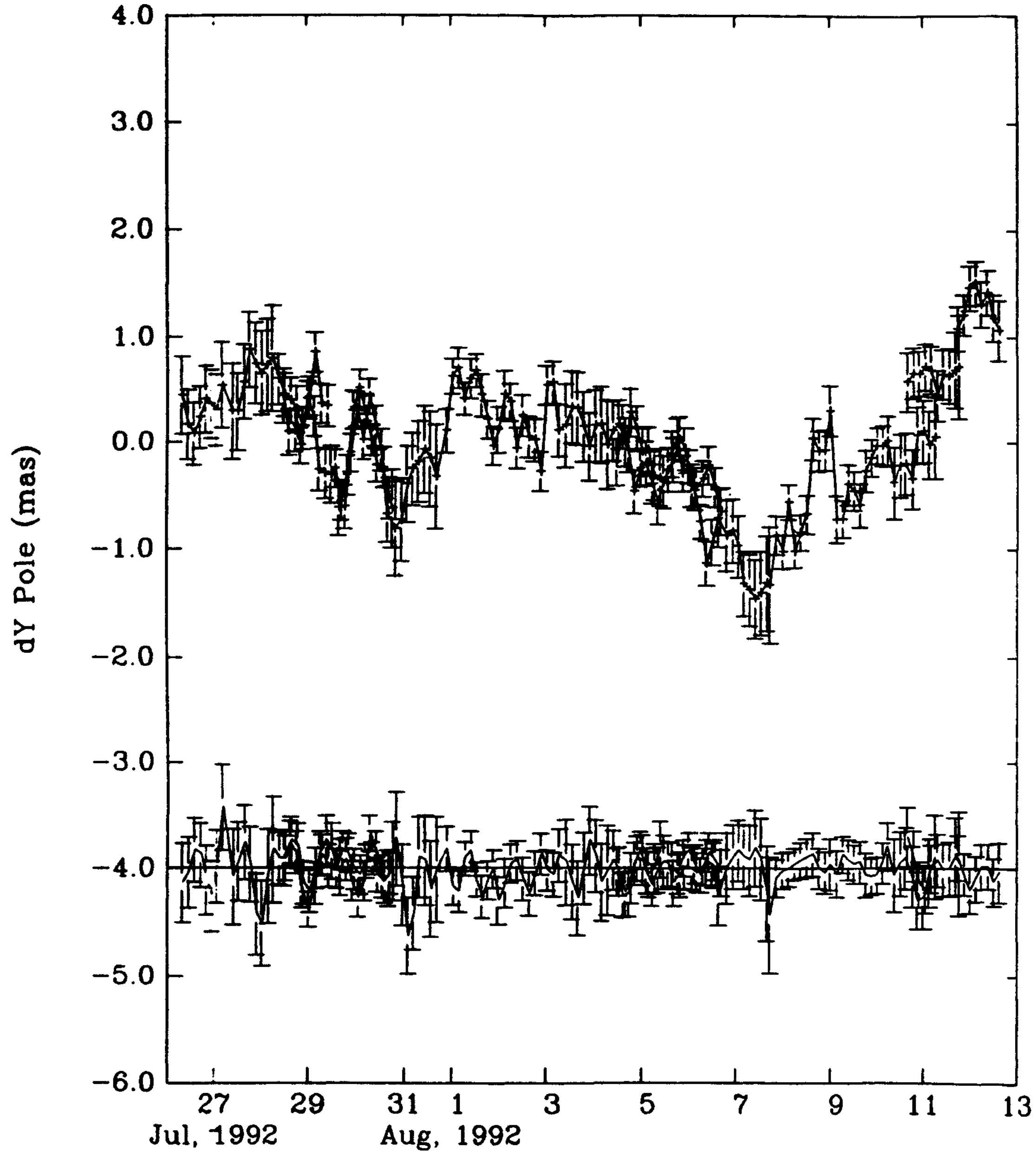

Figure 5. Same as Figure 4 except Y-pole position differences are shown.

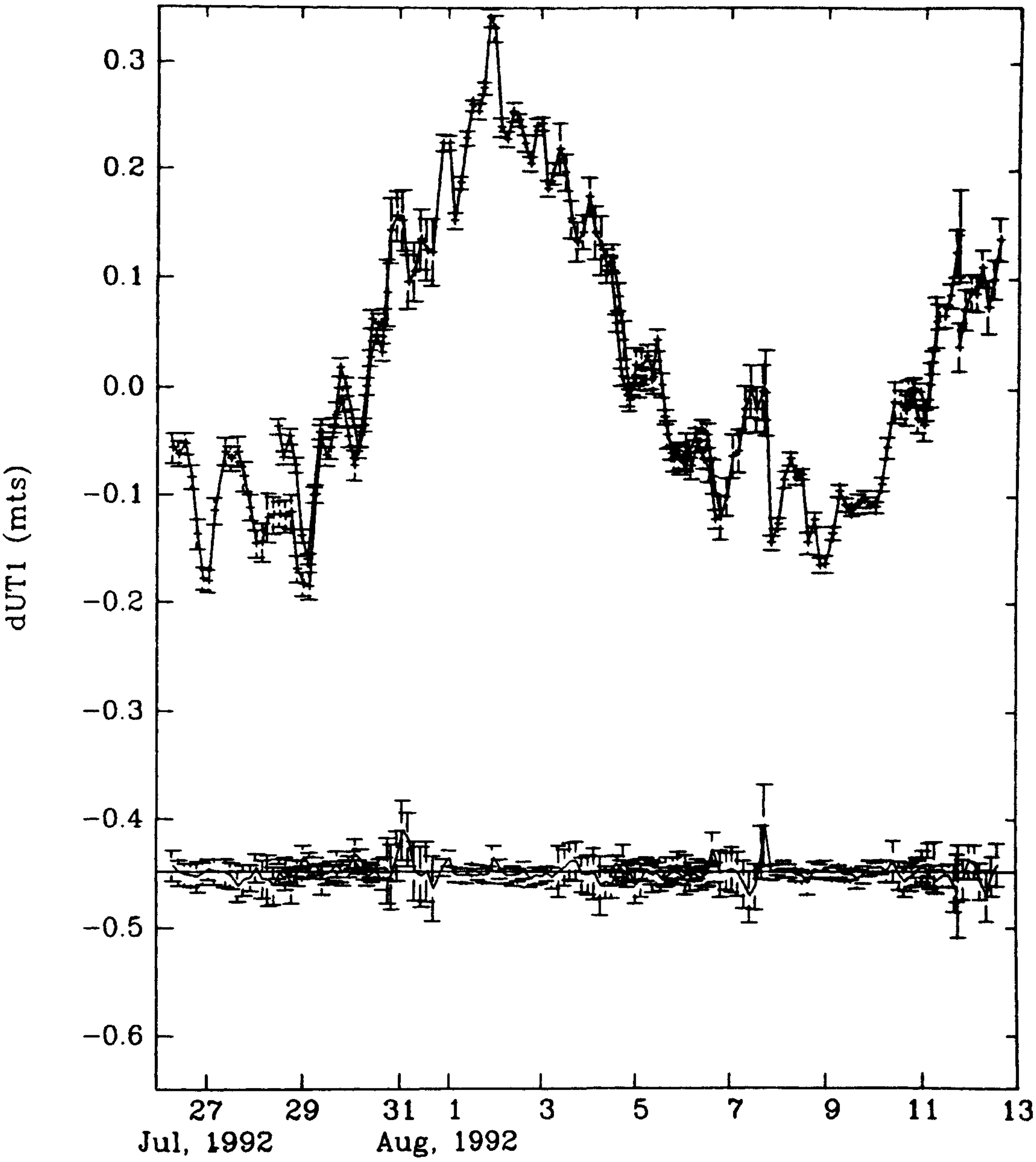

Figure 6. Same as Figure 4 except UT1-AT differences are shown.

UNIVERSAL TIME DERIVED FROM VLBI, SLR AND GPS

D.Gambis, N. Essaifi, E.Eisop and M. Feissel

Universal Time solution combined by IERS from individual series is mainly based on VLBI inertial techniques. Although satellite methods like SLR or GPS have reached a remarkable precision, they do not give access to a highly accurate non-rotating reference frame, which restricts the possibility of determining directly UT1 from their data processing. This is mainly due to uncertainties in the even zonal harmonics of the gravity field and in various models (ocean tides). We show here that it is still possible to combine the high-frequency fluctuations contained in GPS "UT1" series with the long-term variations in the VLBI solution to derive a mixed UT1(VLBI+GPS) solution of great interest for its accuracy, time resolution but also for its economic advantage.

INTRODUCTION

By 1988, GPS had shown its ability to monitor polar motion. As a result IERS decided to include this technique as a part of its activities. After IGS'92 campaign extending from June through September 1992, five analysis centers continued their work on a routine basis. IERS has recently begun to incorporate these data in its regular analyses. In addition to the pole components estimation some analysis centers, CODE, JPL, ESOC and EMR [1,2] are also computing an internal "UT1" series or a derived quantity (*e.g* the excess to 86400 s of the length of the day, LOD). Due to the fact that satellite methods are not inertial the celestial reference system they define is not stable over long periods of time; this prevents the satellite technique to accurately determine long-term UT1 variations. We show in the present paper that their high-frequency signal is still valuable when associated to the long-term variations of UT1 VLBI series.

DATA USED IN THE ANALYSES.

Four GPS analysis centers currently derive UT1-UTC (or LOD values). The present sudy is only concerned by UT1 for Earth orientation purposes, consequently, LOD series given by JPL and ESOC have been integrated to give a "UT1" series. Because of missing values or gaps in some series, interpolation was required to derive continuous and homogeneous "UT1" series. Due to large jumps in the data, the analysis was made on a restricted interval for EMR. The characteristics of each series are listed on table 1. Other operational series used in the analyses and/or in the comparisons are also listed.

	int. (d)	sampl. (d)	1992 June	Sept.	1993 Jan.	March
GPS						
EOP(CODE) 92 P 04	1	1				
EOP(JPL) 92 P 02	1	1				
EOP(JPL) 92 P 03	1	1				
EOP(ESOC) 92 P 02	1	1				
EOP(EMR) 92 P 04	1	1				
VLBI						
EOP(NOAA) 93 R 01	3	1				
EOP(NOAA) 93 R 03	1	0.1				
SLR						
EOP(CSR) 91 L 01	3	3				

Table 1 - GPS, VLBI and SLR Universal Time available at IERS/CB as of 15 March 1993

Differences between the "UT1" series for each GPS center and an external reference like the IERS combined solution (EOP (IERS) C 04) show a wide range of errors (Fig. 1) mainly linked to inaccuracy in the celestial frame defined in orbit computation. Fig.2 shows the geometrical configuration of the satellite orbit relatively to the various reference frames implied. Due to mismodeling in the even zonal harmonics of the gravity field, to ocean tides and also to atmospheric gravitational effects linked to pressure variations, the node longitude and consequently UT1 (hour angle, reckoned from the prime meridian, of a point on the celestial equator)[3] are affected by long-term errors. This prevents the satellite technique to accurately determine long-term UT1 variation. Some analysis centers like CSR have solved this problem by using external a-priori VLBI values in their computations[4].

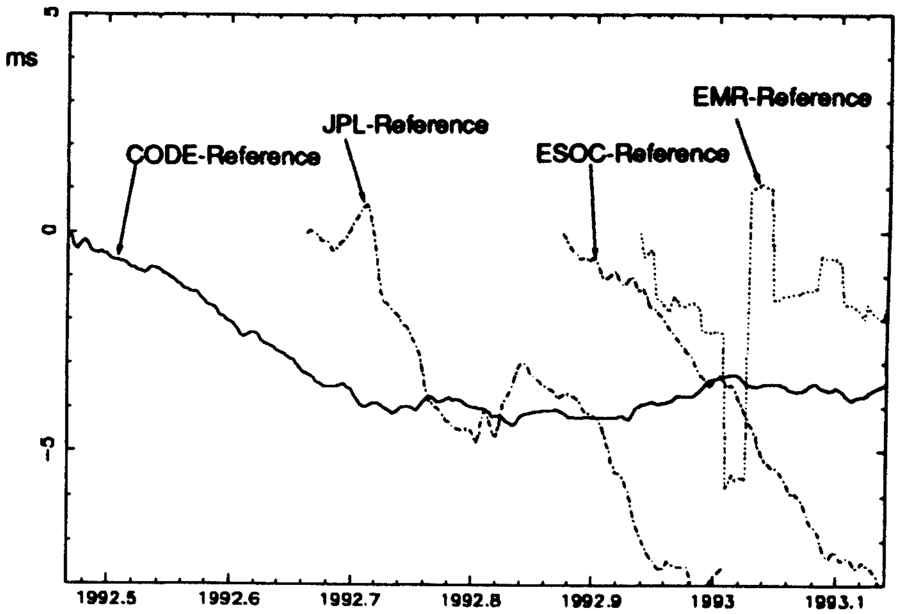

Fig. 1 - Raw "UT1" (or integrated values of LOD for JPL and ESOC) derived from GPS analysis present large systematic low-frequency errors relatively to external series (IERS combined solution) which prevents their direct use in current analyses. The plotted differences are arbitrarily set to zero at the start of the time series.

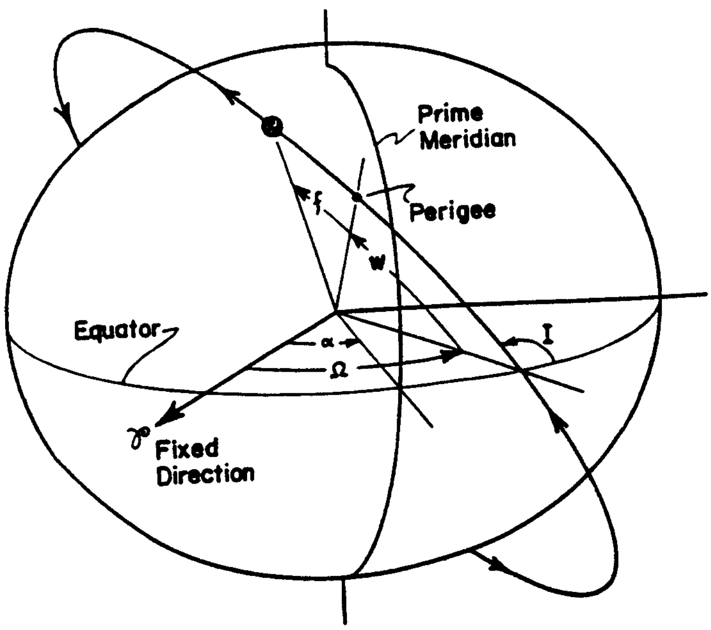

Fig. 2 - Representation of the orbit configuration relative to various reference frames. α : angle proportional to UT1 is obviously correlated to Ω, longitude of the ascending node of the satellite orbit; its determination suffers from mismodeling of Ω.

CONSTRUCTION OF A UT1 SERIES BASED ON GPS AND VLBI SOLUTIONS

We want to set up a procedure of constructing a mixed UT1 series involving long-term VLBI variations of EOP(NOAA) 93 R 01 associated to high-frequency variations given by GPS analysis *e.g.*UT1(VLBI+GPS) the most simple possible for clarity of the process. High frequency terms are removed in VLBI series while they are kept for internal GPS "UT1" series. The critical point concerns the threshold determination within which the high-frequency information contained in the GPS series is valuable. The criteria we have chosen is the following:

Parallel periodograms are made for CODE, JPL and the VLBI solutions. Depending on the analysis center (CODE or JPL) the agreement is fair until a specific period (respectively about 80 and 30 days) which is the threshold corresponding to the optimal filtering (Fig.3). This analysis could not be done for ESOC and EMR because of the relatively short data interval available.

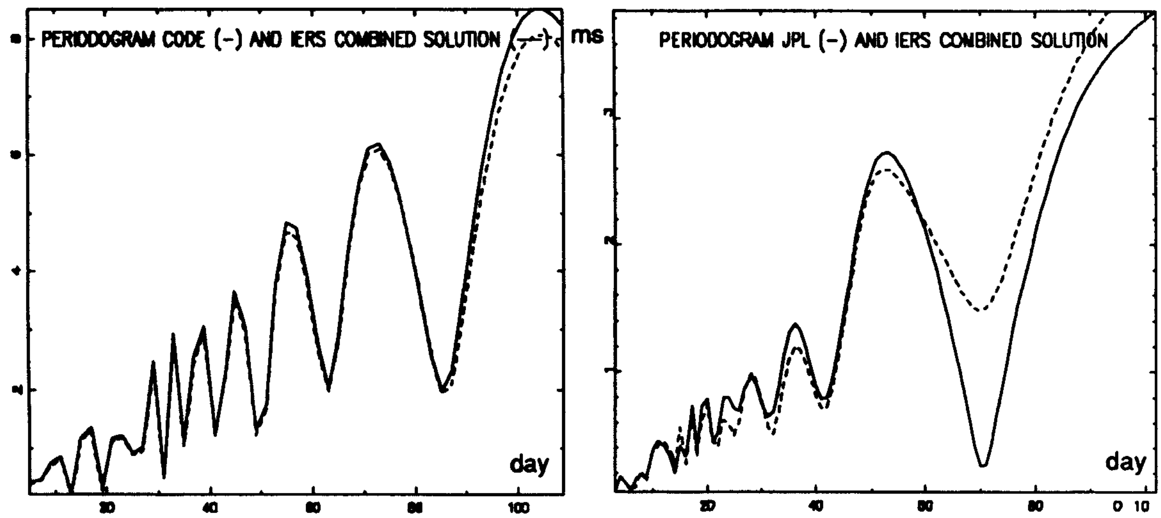

Fig. 3 - Periodograms of raw "UT1" GPS series compared to those of EOP(NOAA) 93 R 01. This analysis gives the threshold for smoothing characteristics determination

COMPARISONS OF UT1(VLBI+GPS) WITH VLBI AND SLR SERIES

In order to estimate the precision of the obtained mixed UT1(VLBI+GPS) solution comparisons with various series have been made. Fig. 4 shows its difference with NOAA and CSR solution; the rms differences of the three series are of the same order. Fig. 5 shows the differences between the mixed UT1(VLBI+GPS) solution and VLBI (EOP(NOAA) 93 R 01) and SLR (EOP(CSR) 91 L 01).

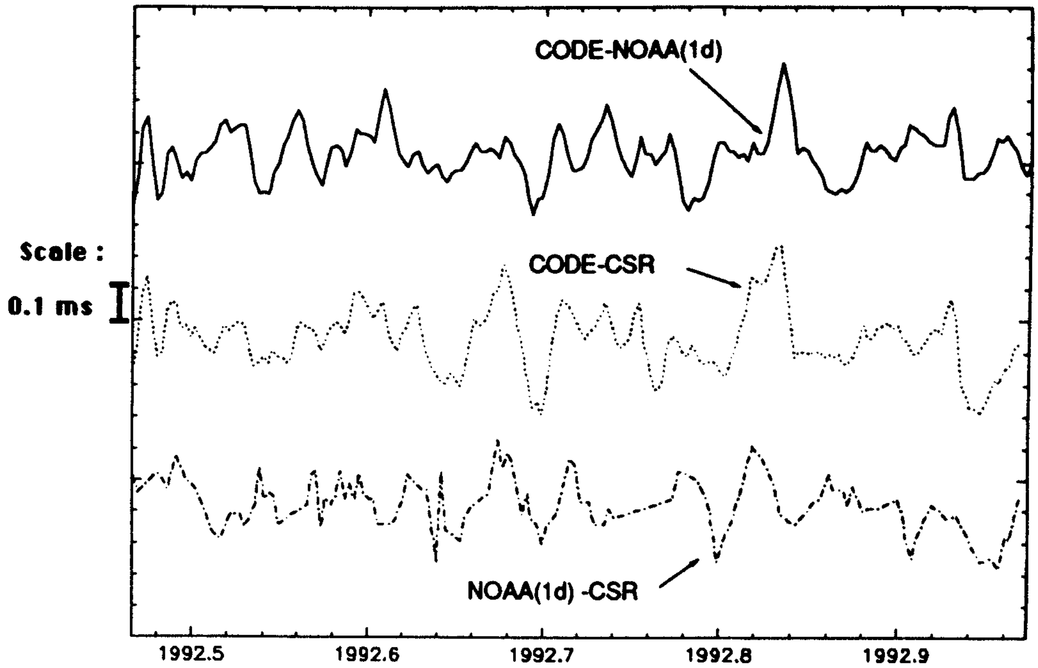

Fig. 4 - Differences between UT1(NOAA+CODE) solution with respectively EOP(NOAA) 93 R 01 and EOP(CSR) 91 L 01. RMS of the three series give estimation of the precisions.

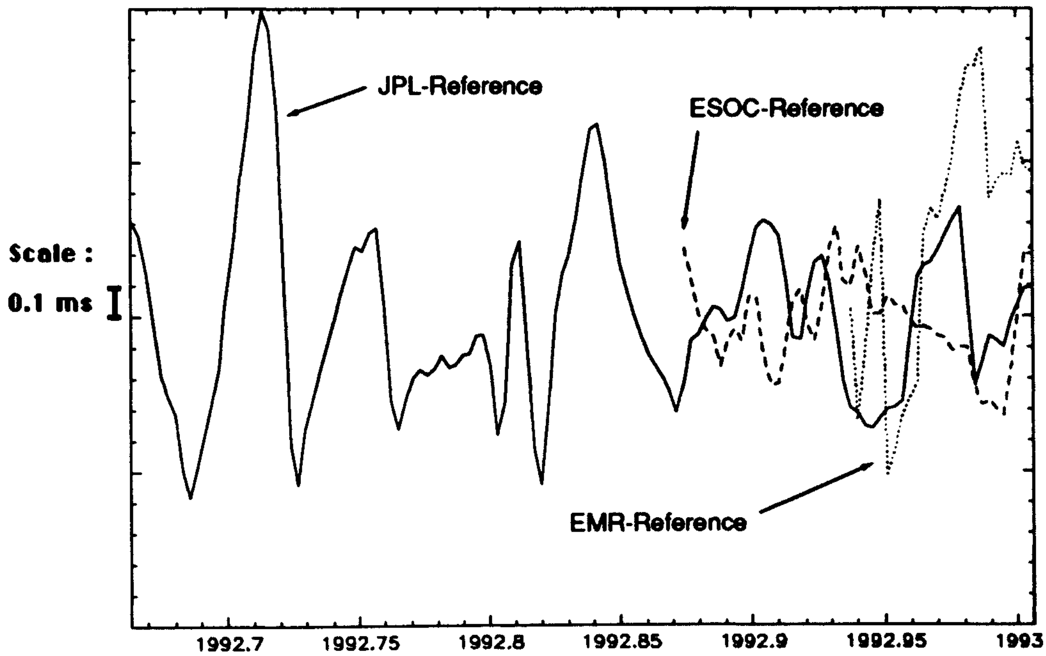

Fig. 5 - Differences between UT1(GPS+NOAA) solutions with an external reference (here EOP(IERS) 90 C 04).

Table 2 gives an estimation of the precision of each series by comparison to EOP(IERS) 90 C 04. These values are only indicative, the combined IERS solution being dependant on VLBI and SLR series.

Series		UT1 (0,0001s)
GPS		
	UT1(NOAA+CODE)	0.81
	UT1(NOAA+JPL)	2.80
	UT1(NOAA+ESOC)	1.47
	UT1(NOAA+EMR)	3.87
VLBI		
	EOP(NOAA) 93 R 02	0.41
	EOP(NOAA) 93 R 03	0.64
SLR		
	EOP(CSR) 91 L 01	0.73

Table 2 - RMS differences of various series with EOP(IERS) 90 C 04.

CONCLUSIONS

Although the internal UT1 series derived from GPS determinations are not directly usable for Earth Orientation monitoring, its high-frequency information can be used together with an external long-term calibration to derive a combined UT1(VLBI+GPS) solution which may be used both for scientific and operational purposes. Outside its high accuracy comparable to other series (NOAA, CSR) the advantage is its high sampling contribution (sub-diurnal) and also, what is not negligible its low production price due only to an additional effort in analyses. Moreover, monthly VLBI contribution seems sufficient to ensure long-term stability of the solution. Refinements of the data analyses are assumed to improve the results in a near future.

REFERENCES

[1]- Annual Report for 1991.

[2]- IGS'92 campaign, IERS Reports.

[3]- IERS Technical note 8

[4]- Aoki S.,Guinot B., Kaplan K.H.,Kinoshita H.,McCarthy D.D. and P.K. Seidelman, 1982, *Astron. Astrophys.*,105,359-361.

SUB-DAILY EARTH ROTATION DURING EPOCH '92

A. P. FREEDMAN, R. IBANEZ-MEIER, J. O. DICKEY, S. M. LICHTEN
Jet Propulsion Laboratory
California Institute of Technology
Pasadena, California 91109

T. A. HERRING
Department of Earth, Atmospheric, and Planetary Sciences
Massachusetts Institute of Technology
Cambridge, Massachusetts 02139

ABSTRACT. Earth rotation data were obtained with GPS during the Epoch '92 campaign in the summer of 1992. About 10 days of data were acquired from 25 globally distributed stations and a constellation of 17 GPS satellites. These data were processed to estimate UT1 corrections every 30-minutes, then smoothed to form a UT1 series with 3-hour spacing. Earth orientation data during Epoch '92 were also obtained by several VLBI groups, and were processed together to yield VLBI estimates of UT1 with 3-hour time resolution. The high frequency behavior of both GPS and VLBI data sets is similar, although drifts between the two series of ~0.1 ms over 2-5 days are evident. Tidally induced UT1 variations from both theoretical ocean models and empirical determinations were compared with the GPS and VLBI series. Estimates of atmospheric angular momentum (AAM) at 6-hour intervals generated by several meteorological centers were also compared with the geodetic data. These comparisons indicate that most of the GPS signal in the diurnal and semidiurnal bands can be attributed to tidal processes, and that UT1 variations over a few days are mostly atmospheric in origin.

1. Introduction

Variations in the rate of rotation of the solid Earth result both from torques applied to the Earth from the exterior or interior and from mass redistributions within the Earth. For high-frequency Earth rotation variations, defined here as rotation rate changes occurring over time scales of a week or less, the principal forces on the solid Earth are thought to come from the atmosphere and oceans. In particular, tidal forcing of the oceans is expected to dominate the rotational variations at periods of one day and less.

A variety of techniques have historically been used to monitor the rotation of the Earth, but only over the past few years has the capability for daily and even sub-daily monitoring of Earth rotation with the requisite precision become available. Current high-precision techniques include very long baseline interferometry (VLBI), satellite laser ranging (SLR), lunar laser ranging (LLR), and, most recently, the Global Positioning System (GPS). VLBI estimates of Earth's rotation angle (UT1 – UTC) at daily intervals and SLR estimates at roughly 3-day intervals have been made for several years. Over the past four years, measurements of UT1 variations with hourly or so time resolution have been made sporadically by both VLBI and GPS techniques [1, 2].

In association with the International GPS Geodynamics Service's (IGS) proof of concept campaign for the summer of 1992, an additional campaign known as SEARCH '92 (Study of Earth-Atmosphere Rapid Changes) was held to monitor high-frequency Earth orientation variations utilizing all space geodetic techniques and to advocate for and facilitate the collection of the best available related geophysical data [3]. Data from a variety of complementary techniques providing a good level of redundancy were acquired, in particular, during the intensive two-week period known as Epoch '92. In this paper, we present GPS estimates of sub-daily variations in UT1 during Epoch '92 and compare these results with a number of these other related data sets. This intercomparison should provide a robust estimate of Earth's true rotational variations at time scales as short as a few hours, and should help as well to improve strategies for processing GPS data.

2. Data sets

2.1. GPS

The GPS data processing strategy is a version of that discussed elsewhere using the JPL GIPSY/OASIS II software [4, 5] and is summarized in Table 1 [see also Zumberge et al., this volume]. Data from a network of 25 stations using a GPS constellation of 17 satellites were acquired over more than 10 days during the last week of July and first week of August, 1992. Owing to the use of anti-spoofing (AS) signal encryption over the weekend, these data are not continuous but are divided into two groups from which two multi-day GPS orbit arcs were created. Corrections to a nominal UTPM series (derived from the IERS Bulletin B) were obtained from the data, with UT1 estimated every 30 minutes and polar motion every two hours. UT1 was modeled as a Gauss-Markov (AR1) process with a steady-state sigma of 0.06 ms and a time constant of 4 hours. Thus, over 30 minutes, 0.028 ms of process noise was added.

Table 1. GPS ESTIMATION STRATEGY

Estimated parameters	
Station locations (8 fiducial sites)	Wet zenith troposphere (random walk)
Satellite states	Clock biases (white-noise)
Solar radiation pressure	Carrier phase biases
UT1 (AR1)	Polar motion (white noise)
Standard models	
Solid Earth tides and equilibrium ocean tides from Yoder et al.[6]	
Gravity field coefficients: GEMT3, 8x8 truncation	
Nutation model: 1980 IAU model	
A priori and fiducial site locations ITRF 91	
Nominal UTPM from IERS Bulletin B	
Rogue receivers: Pseudorange (1-meter), Carrier Phase (1 cm)	
6-minute data interval (obtained by decimation)	

We generated UT1 time series using a variety of orbit modeling strategies [Zumberge et al., this volume]. Our preferred strategy employed multi-day orbit arcs wherein one set of satellite states (positions and velocities) was estimated for each satellite. Three stochastic solar radiation parameters for each satellite were modeled as AR1 processes and estimated every hour. Alternative estimation strategies yield UT1 series that differ, but the results and conclusions described below do not significantly change if these other UT1 series are used.

For comparison with the VLBI data, we constructed a smoothed GPS UT1 data set by applying a Gaussian filter with a half-width of about one-half hour to smooth the 30-minute data and interpolate them to the epochs of the VLBI data. Although it contains GPS-derived UT1 measurements every 3 hours, this smoothed data set is not identical to a 3-hour GPS solution, since the latter contains UT1 values averaged over a 3-hour window whereas the former is effectively smoothed over a 1- to 2-hour window.

2.2. VLBI

VLBI data were acquired from the three networks described in Table 2. Note that on certain days, UT1 was measured by more than one VLBI network, enabling an estimate of the quality of the VLBI data. The correlated VLBI data were combined using the MIT Kalman filter programs CALC/SOLVK. UT1, polar motion, nutation corrections, and station troposphere parameters were estimated over 24 hour time spans, with UT1, polar motion, and the troposphere parameters modeled as random walks [see Herring, this volume].

Several solutions were generated in which UT1 was estimated either every 30 minutes or every 3 hours. The 30-minute solutions were rather noisy, so a 3-hour series, in which UT1 was estimated every 3 hours with 0.04 ms sigma resets after a diurnal and semidiurnal a priori tide model had been applied, was used in this study. A final smoothed VLBI solution was generated in which the 24-hour data sets from all the networks were combined using a mild Gaussian filter.

Table 2. VLBI DATA

NASA's Goddard Space Flight Center (GSFC) – NASA R&D
8 experiments, 5-6 sites in N. America, Hawaii, and Europe
National Oceanic and Atmospheric Administration's (NOAA) Laboratory for Geosciences – IRIS
4 experiments (one mobile, three IRISA), 5 sites in N. America and Europe
Unites States Naval Observatory (USNO) – NAVNET
6 experiments, 4-6 sites, located around globe

Data run from July 26 through August 11. Four days have measurements by both NAVNET and NASA R&D. Each experiment can have significantly different formal errors.

2.3. TIDE MODELS

A variety of additional data sets were used in evaluating the GPS and VLBI time series. Two models for tidally-induced diurnal and semidiurnal UT1 variations were compared, one based on theoretical ocean models [7] and one empirically derived from many years of measured UT variations [8]. The theoretical series, referred to as the Gross tide model, is based on the oceanic angular momentum model of Seiler [9]. This formulation also contains corrections to the standard tide model [6] for non-equilibrium ocean tides at fortnightly and monthly periods. The empirical model, referred to as the Herring tide model, is based on 8 years of VLBI data. It contains estimates of the diurnal and semidiurnal tidal terms only. Note that this empirical tide series may contain additional diurnal signals other than those due to the non-equilibrium ocean tides, such as the effects of atmospheric tides. Both tidal UT1 series may be compared directly to geodetic UT1 estimates.

2.4. AAM 6-HOURLY DATA

If angular momentum were exchanged solely between the atmosphere and the solid Earth, atmospheric angular momentum (AAM) variations would result in corresponding changes in the length of the day (LOD), the time derivative of UT1. Several sets of AAM were computed every 6 hours as part of the SEARCH/IGS effort by three meteorological centers: the U. S. National

Meteorological Center (NMC), the European Centre for Medium-Range Weather Forecasts (ECMWF), and the Japanese Meteorological Agency (JMA). For each center, the AAM quantity that we use consists of the χ_3 AAM wind term integrated to the top of the model atmosphere (either 50 mbar or 10 mbar, depending on center) plus the full pressure (not inverted-barometer) term. Gaps in the AAM series were filled by linear interpolation.

We used these data sets to estimate atmospherically induced variations in UT1. Since AAM is a substitute LOD, the AAM series must be integrated to be compared to a UT1 series. However, two arbitrary constants, effectively a bias in LOD and a bias in UT1, enter into this integration. For the comparisons shown below, linear models are removed from the AAM and geodetic UT1 series to account for these constants.

2.5. SMOOTHED REFERENCE SERIES

A reference series, based on the IERS Bulletin B nominal values used for the GPS analysis, was used to remove long-period UT1 variations. Note that all the geodetic series shown have the shorter-period (<35 day) tides explicitly removed according to the standard Yoder et al. [6] model, while subtracting the nominal UT1R series effectively removes the longer period terms of [6].

3. Results

3.1. GPS VS. VLBI

We have compared the GPS-derived UT1 with VLBI estimates of UT1 – TAI for each network-day of data. UT1 was estimated every 30 minutes in both sets of data. Typical formal errors of the various time series are summarized in Table 3. We present below only results for the smoothed and interpolated sets of VLBI and GPS data. These two data sets are shown in Figure 1. For display purposes, the UT1 values have been differenced with the IERS Bulletin B reference series. The bias between GPS and VLBI is arbitrary. Note the gap in GPS data due to the use of AS during the weekend of August 1-2 which precludes the construction of a continuous two-week long GPS time series. The 6-day time span at the end of July where data exist from both techniques is referred to below as period A, while the 4.5-day time span in August is referred to as period B.

Although there appears to be a drift between the two series over several days, their diurnal variability is similar. If the two series are differenced, linear trends can be fit separately to periods A and B to quantify both the drift and residual scatter in GPS minus VLBI. These values are given in Table 3. Over 4 to 6 day time spans, the GPS shows a fairly linear drift with respect to VLBI, with drift rates of ±20-40 μsec/day. After removing these drifts, the total RMS scatter of GPS minus VLBI UT1 is 0.023 ms. These drifts are probably a result of drift in the GPS time series caused by systematic effects such as orbit mismodeling.

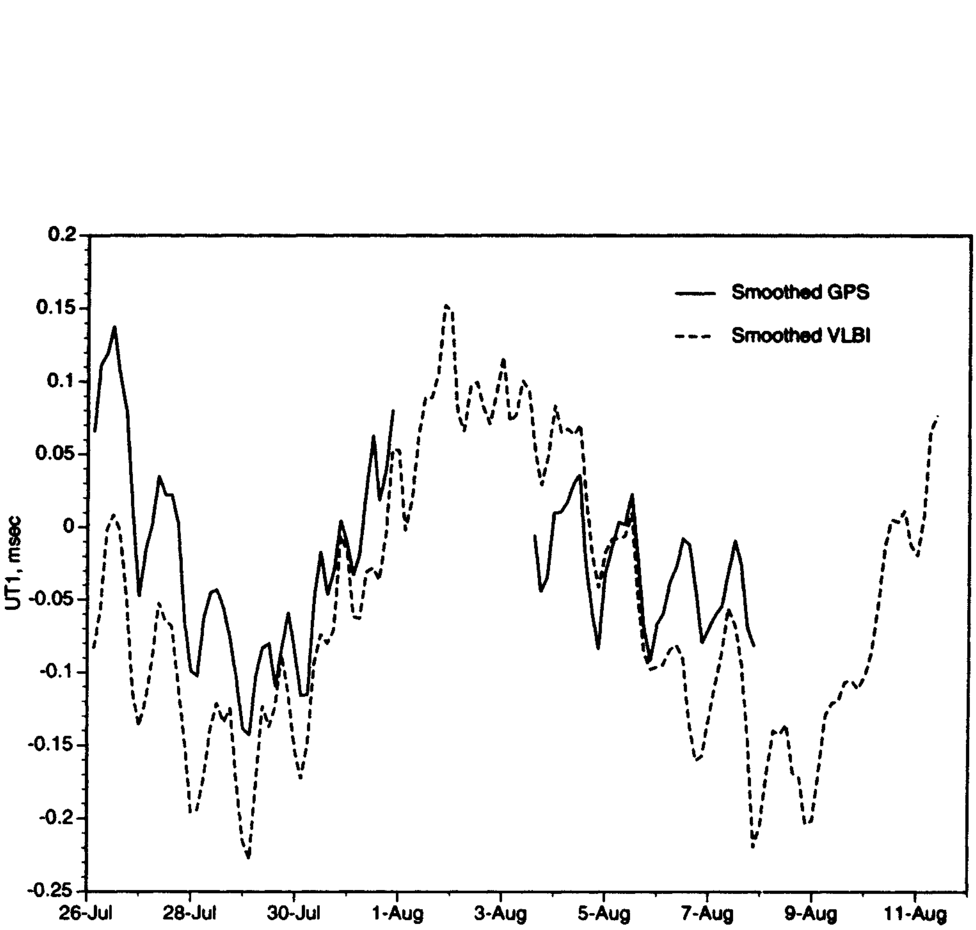

Fig. 1. UT1 from GPS and VLBI evaluated every 3 hours.

Table 3. STATISTICS

	Typical 30-Minute UT1 Formal Errors		
GPS	**IRIS VLBI**	**NAVNET**	**NASA R&D**
0.02-0.03 ms	0.02-0.04 ms	0.015-0.04 ms	0.01-0.025 ms
	GPS Minus VLBI		
	Period A	**Period B**	**Entire time span**
Slope	-0.018 ms/day	0.041 ms/day	--
RMS scatter	0.022 ms	0.026 ms	0.023 ms
	GPS Minus Tides		
	GPS UT1 only	**GPS minus Herring**	**GPS minus Gross**
RMS Scatter	0.032 ms	0.018 ms	0.035 ms
	UT1 Minus (AAM+Tides)		
RMS of difference	**NMC AAM**	**ECMWF AAM**	**JMA AAM**
GPS UT1	0.021 ms	0.022 ms	0.019 ms
VLBI UT1	0.027 ms	0.022 ms	0.022 ms

The relationship between GPS and VLBI may be further explored by computing power spectra of the GPS and VLBI UT1 and their difference (Fig. 2). Power spectra were obtained separately for the two periods A and B (after padding with zeros to the same length) and averaged together. A 3-point spectral smoothing was used (corresponding to a bin width of 0.375 cycles per day). Both the VLBI and GPS series show similar power in the diurnal and semidiurnal bands. Differencing the two removes the peaks in power at both frequencies, suggesting that there is a true geodetic signal in these bands that is accurately sensed by both techniques. This signal is for the most part tidal in origin, as shown below.

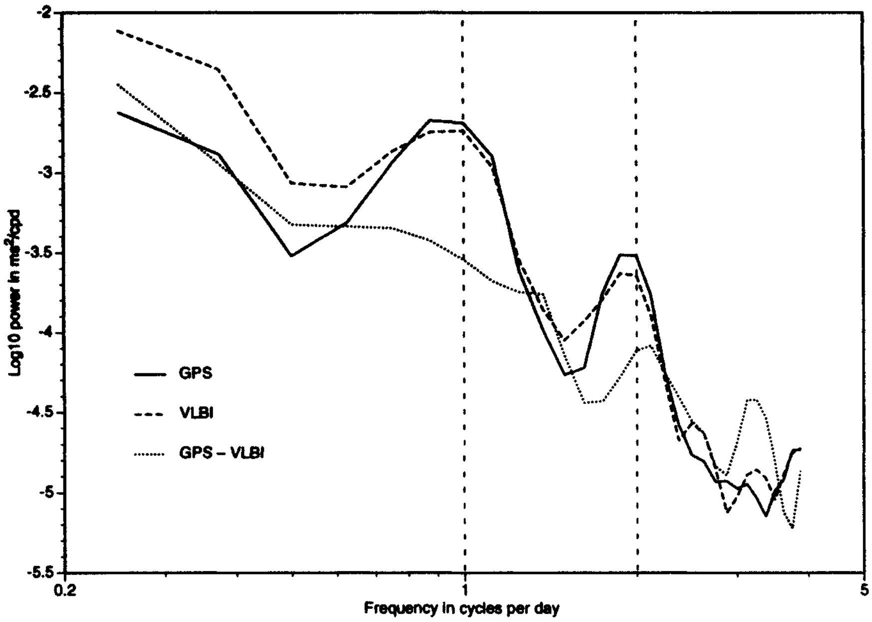

Fig. 2. Power spectra of the GPS and VLBI UT1 series and their difference.

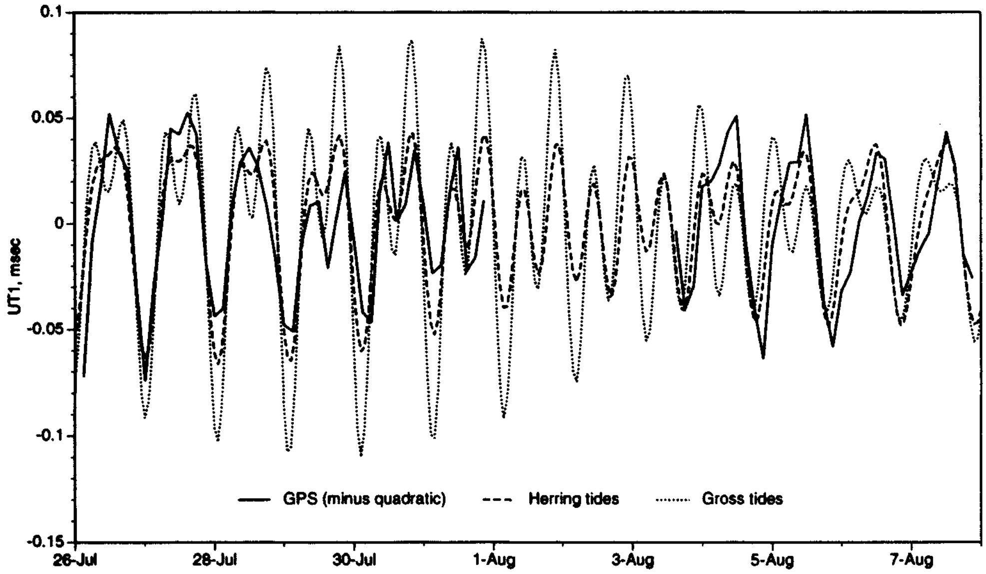

Fig. 3. GPS UT1 compared to two models of tidally induced UT1 variations.

3.2. GPS VS. TIDES

In Figure 3, we compare the smoothed GPS UT1 to the two models of tidally-induced UT1 variations. The GPS series for each period (A and B) has had a best-fitting quadratic subtracted to remove longer-period fluctuations, thus making the residual series easy to compare with the tides. Note that the Herring, empirical model more accurately reflects the observed UT1 variability than does the Gross, theoretical model.

These differences can again be described through the use of power spectra. Power spectra (computed as before) of the GPS UT1 series and the GPS series minus the two tide models are shown in Fig. 4. The Herring model removes most of the excess power in the diurnal and semidiurnal bands, with a hint of signal remaining at 2 cycles per day (cpd). The Gross model removes some power at diurnal frequencies, but adds substantial power at semidiurnal frequencies (consistent with the large amplitudes seen in Fig. 3). These differences are quantified in Table 3, which shows the RMS scatter of the three time series whose power spectra are plotted in Fig. 4. The Herring model appears to more accurately reflect the actual UT1 variations at diurnal and semidiurnal frequencies. Reasons for this may include inaccuracies in the theoretical ocean models and additional non-oceanic signal at these frequencies.

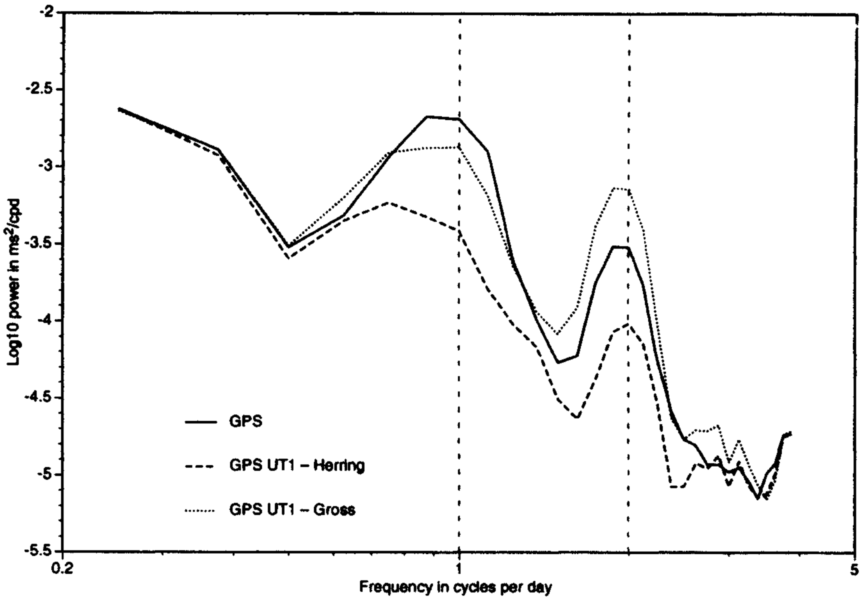

Fig. 4. Power spectra of the GPS UT1 series and the GPS series differenced with each of the two tide models.

3.3. GPS VS. AAM

The three series of atmospheric angular momentum (AAM) values evaluated every 6 hours provided by the NMC, the ECMWF, and the JMA are shown in Fig. 5. The variations in each series over periods greater than 1 to 2 days are similar, but the higher frequency fluctuations do not appear to be common among the three. The biases between the series are real, and come from differences in the meteorological models of the centers.

Since AAM represents a form of LOD, the curves in Fig. 5 must be numerically integrated to generate UT1 series whose variations are implied by the AAM. These series are shown in Figure 6. Also shown are a GPS UT1 series and the UT1 variations expected from the longer-period (14 and 30-day) non-equilibrium ocean tides emerging from the numerical ocean model [7]. Each series for each of periods A and B has had a best-fitting linear bias and trend removed. Since the ECMWF series for period A starts on July 27 and thus is one day shorter, it has had a trend removed which minimizes the differences between the ECMWF curve and the other two AAM curves. The three integrated AAM curves show similar behavior for period A, with more contrasting forms for period B. All the AAM curves appear consistent with the overall shape of the GPS UT1 curve. The longer-period tide corrections do not add substantial signal at these few-day periods.

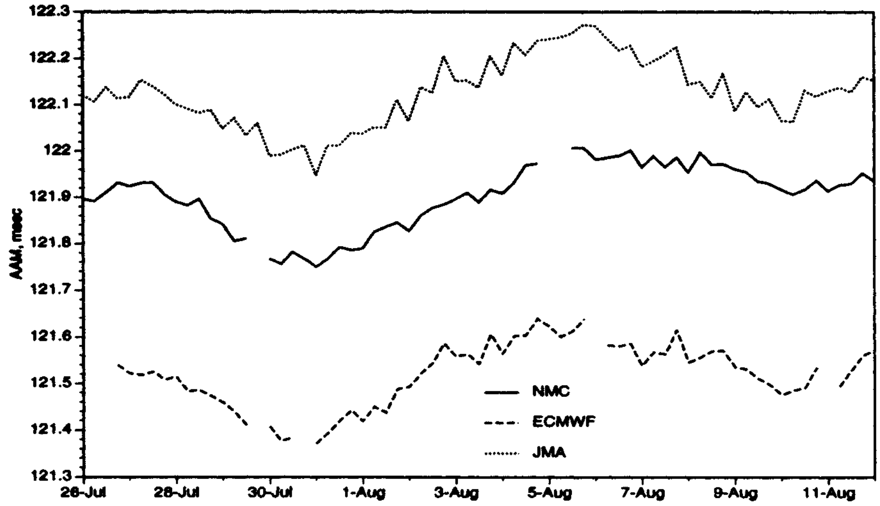

Fig. 5. Three series of atmospheric angular momentum (AAM) values.

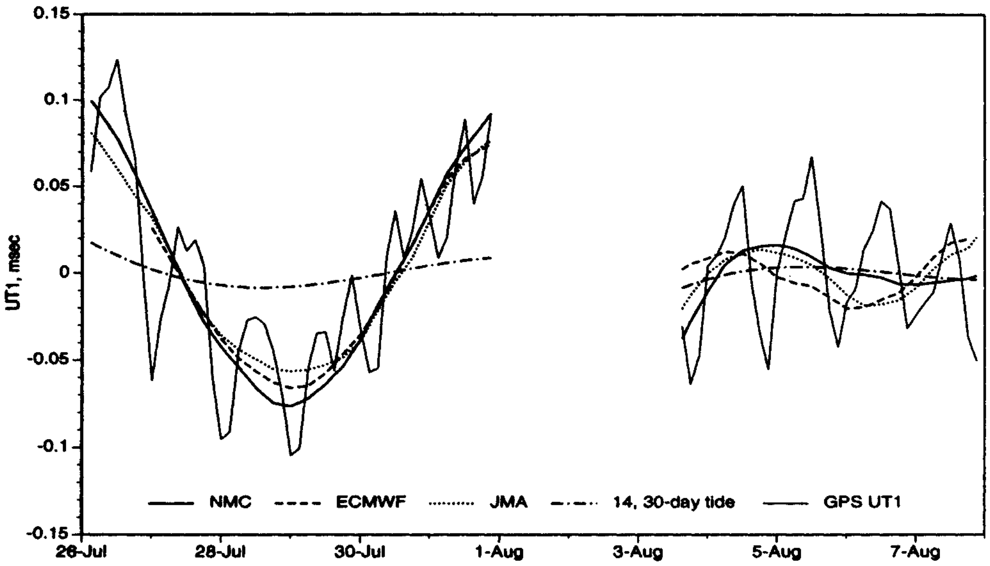

Fig. 6. Comparison of integrated AAM with geodetic UT1 variations.

The sum total of the integrated AAM, diurnal and semidiurnal tides (from [8]) and longer-period tides (from [7]) are shown in Figure 7, together with the observed UT1 variations from GPS and VLBI. Linear trends were removed from each series for each period. Most of the geodetic signal can be described by the sum of AAM variations and tidally induced UT1, with the tides acting at periods of one day and less and AAM acting at periods greater than a day. The differences between GPS and VLBI are at least as large as those between the AAM series themselves and the AAM and geodetic series. Thus, no center or technique stands out as superior. The RMS of the differences between the geodetic and AAM+tides series are shown in Table 3; all are consistent with the typical GPS and VLBI formal errors of 0.02-0.03 ms.

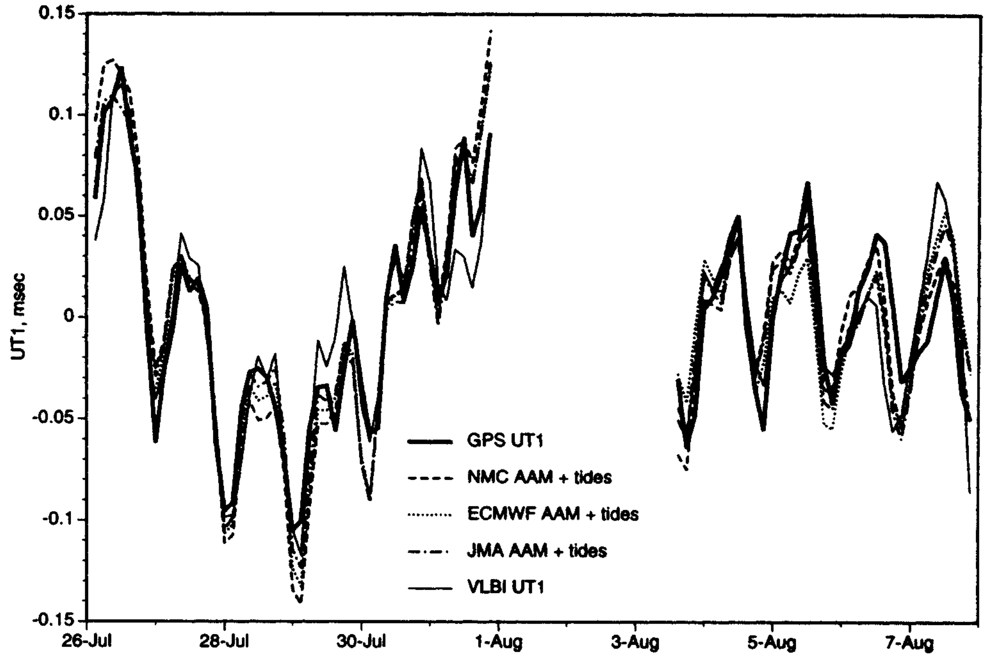

Fig. 7. The sum of the integrated AAM and diurnal, semidiurnal, and longer-period tides compared with the observed UT1 variations from GPS and VLBI.

4. Conclusions

Differences between the various series considered here tend to be at the level of 0.02 to 0.03 ms. These RMS differences are consistent with the formal uncertainties of the data themselves. The main exception is the theoretical tide model, which simply does not yield the signal seen geodetically. There is also a drift in the GPS data relative to VLBI which, over time spans of 6 days or so, appears to be linear but with a non-unique drift rate.

Both GPS and VLBI exhibit nearly identical variability in the diurnal and semidiurnal bands, attributable to tidal variations whose values are well derived from many years of geodetic VLBI data. There is no residual signal in these frequency bands that exceeds the level of formal error of the data, although residual signals with amplitudes smaller than 0.02 ms could certainly be present. Although the theoretical tide model does not agree with observations in either band, the disagreement is largest in the semidiurnal frequency band.

The multi-day variability of AAM from all the meteorological centers is similar, and yields AAM-derived UT1 curves that are consistent with the variability of the geodetic UT1 at periods longer than one day. At diurnal and shorter periods, however, the AAM centers generate inconsistent estimates. Moreover, the sub-daily variability of the AAM is quite small and cannot, at this point, be disentangled from oceanic tidal effects and noise in the geodetic data. However, limits can be placed on the size of any residual AAM signal.

Thus the signal seen in the GPS time series can be represented by the sum of four effects: tides at diurnal and semi-diurnal periods, AAM fluctuations at periods of one to at least several days, a linear drift in UT1 due possibly to orbit mismodeling, and a high-frequency noise component. To accurately solve for UT1 with GPS at these frequencies, the tidal variations in UT1 must certainly be modeled, either by explicit use of the Herring tide model, or by allowing adequate variability in the estimated UT1. AAM-induced variations are slow enough that if UT1 (or LOD) is estimated at least daily, this variability need not be explicitly modeled. Further research is necessary to investigate and reduce both the drift in UT1 of ~0.1 ms over 2-5 days, and the level of high-frequency noise present in the data.

ACKNOWLEDGMENTS. The authors thank and acknowledge the cast of literally thousands who were involved in collecting and processing the vast quantities of data from both GPS and VLBI, as well as the people and institutions involved in generating the AAM data sets. The work described in this paper was carried out by the Jet Propulsion Laboratory, California Institute of Technology, under contract with the National Aeronautics and Space Administration.

References

[1] Herring, T. A., and D. Dong, "Current and Future Accuracy of Earth Rotation Measurements," in *Proceedings of the AGU Chapman Conference on Geodetic VLBI: Monitoring Global Change (Washington DC, April 22-26, 1991)* pp. 306-324, NOAA Technical Report NOS 137 NGS 49, NOS/NOAA, Rockville, MD, 1991.

[2] Lichten, S. M., S. L. Marcus, and J. O. Dickey, "Sub-Daily Resolution of Earth Rotation Variations With Global Positioning System Measurements," *Geophys. Res. Lett.*, **19**, 537-540, 1992.

[3] Dickey, J. O., "High Time Resolution Measurements of Earth Rotation," in *Advances in Space Research*, Pergamon, in press, 1994.

[4] Lichten, S. M., and J. S. Border, "Strategies for High-Precision Global Positioning System Orbit Determination," *J. Geophys. Res.*, **92**, 12751-12762, 1987.

[5] Lichten, S. M., "Estimation and Filtering for High-Precision GPS Positioning Applications," *Man. Geod.*, **15**, 159-176, 1990.

[6] Yoder, C. F., J. G. Williams, and M. E. Parke, "Tidal Variations of Earth Rotation," *J. Geophys. Res.*, **86**, 881-891, 1981.

[7] Gross, R. S., "The Effect of Ocean Tides on the Earth's Rotation as Predicted by the Results of an Ocean Tide Model," *Geophys. Res. Lett.*, **20**, 293-296, 1993.

[8] Herring, T. A., and D. Dong, "Measurement of Diurnal and Semidiurnal Rotation Variations and Tidal Parameters of the Earth," *J. Geophys. Res.*, submitted, 1993.

[9] Seiler, U., "Periodic Changes of the Angular Momentum Budget Due to the Tides of the World Ocean," *J. Geophys. Res.*, **96**, 10,287-10,300, 1991.

SUB-DAILY POLAR MOTION DURING EPOCH '92 WITH GPS

R. IBANEZ-MEIER, A. P. FREEDMAN, S. M. LICHTEN, U. J. LINDQWISTER,
R. S. GROSS
Jet Propulsion Laboratory,
California Institute of Technology
Pasadena, California 91109

T. A. HERRING
Department of Earth, Atmospheric, and Planetary Sciences,
Massachusetts Institute of Technology
Cambridge, Massachusetts 02139

ABSTRACT. Data from a worldwide Global Positioning System (GPS) tracking network spanning six days during the EPOCH '92 campaign are used to estimate variations of the Earth's pole position every 30 minutes. The resulting polar motion time series is compared with estimates derived from very long baseline interferometry (VLBI) observations. A time domain comparison of the semidiurnal and prograde diurnal bands yields better than 0.3 milliarcsecond rms differences between the series. Additional comparison with an ocean tidally-induced polar motion model suggests that most of the periodic subdaily variations in the GPS polar motion signal can be attributed to ocean tides.

1. Introduction

Observations of the motion of the pole have a long history [See Lambeck, 1980; Eubanks, 1993, and references therein]. Polar motion, which is the movement of the Earth's rotation axis with respect to its crust, is a dynamic response of the Earth forced by its interactions with other celestial bodies and its own internal dynamics. The location of the rotation axis is given with respect to a crust-fixed, reference point (e.g., the International Earth Rotation Service (IERS) reference pole [McCarthy, 1992]) by using two coordinates, polar motion x (PMX) and polar motion y (PMY), where the x-axis lies along the Greenwich meridian, orthogonal to the reference pole z-axis, and the y-axis lies 90 degrees to the west.

Angular momentum changes in the oceans at daily and sub-daily periods of tidal origin, a product of the response of the world's oceans to the tidal potential at high frequencies, lead to associated diurnal and semidiurnal changes in polar motion [Seiler, 1991; Gross, 1993; Wunsch and Seiler, 1992]. Since the tendency in the polar motion is towards decreasing amplitudes at shorter periods, increasing sensitivity has been necessary to detect these high-frequency pole position changes. Herring et al. [1991] and Lindqwister et al. [1992] obtained GPS daily polar motion estimates in agreement with VLBI at the 0.5 mas (1.5 cm) level or better, and subsequently several GPS processing centers have been routinely reporting daily estimates of pole position as part of the International GPS and Geodynamics Service (IGS). We report here on sub-daily time-domain GPS-based polar motion measurements and their comparison with VLBI. The data were collected during the intensive observing period known as EPOCH '92 (part of the SEARCH '92 Campaign organized by the IERS), during which time continuous and high time resolution data were obtained by both VLBI and GPS.

2. Data Sets and Estimation Strategies

Data from 25 globally distributed GPS Rogue receivers tracking 17 GPS satellites from July 26 through July 31, 1992 were processed with the Jet Propulsion Laboratory's (JPL) GIPSY-OASIS II software. The data arc could not span more contiguous days due to anti-spoofing (AS) signal encryption on August 1-2. The JPL software and standard JPL GPS estimation strategies, incorporating Kalman filtering, are described in detail by Lichten [1990a, 1990b] and Blewitt [1993]. The estimation strategy for this study is described by Zumberge et al. [this volume]. GPS orbit states and three solar radiation parameters corresponding to three orthogonal flux components were estimated for each satellite. Earth orientation parameters were estimated by using the IERS Bulletin B time series as the source for nominal values. Earth rotation (UT1 – UTC) variations were estimated every 30 minutes starting from an initial fixed value by using first-order Markov process updates with a correlation time of 6 hours and a steady-state process noise 1-sigma constraint of 0.06 ms [Freedman et al., 1993, and this volume]. Station geocentric coordinates, except those for up to 8 fiducial (fixed) sites, were estimated as constants over the entire six day period, with ITRF 1991 coordinates [Boucher et al., 1992] used as a priori station locations. As observed by Lindqwister et al. [1992], changing fiducial sites in our estimation strategies induced only bias changes in our polar motion series, consistent with small rigid-body rotations of the reference frame. The pole position variability remained nearly invariant even in the absence of fiducial sites.

Two different estimation strategies for the satellite orbits were employed [see Zumberge et al., this volume]. The strategy which proved superior for polar motion estimation consisted of re-estimating each satellite state (position, velocity and solar radiation pressure coefficients) every 24 hours. The white noise restarts for each GPS satellite were staggered over a 5 hour interval around noon to maintain continuity in the UT1 series. We then tried a variety of estimation strategies for polar motion and found that unconstrained white noise estimates, every 30 minutes or less, gave consistent results in the prograde diurnal and semidiurnal bands discussed below. Typical postfit rms residuals were close to 6 mm for carrier phase and 35 cm for pseudo-range data.

The VLBI series used for comparison in this study was generated from data acquired by three different VLBI networks: "NASA R&D", "IRIS" and "NAVNET" (see Freedman et al. [1993], and Herring [this volume] for more details). UT1, polar motion, nutation corrections, and station troposphere parameters were estimated over 24 hour time spans, with UT1, polar motion and troposphere parameters modeled as random walks. Polar motion was estimated every 2 hours with 1.2 mas 1-sigma resets.

We have also compared our series to a model of tidally-induced polar motion variations. This model, referred to as the Herring tide model [Herring and Dong, 1993], is an empirically determined model based on eight years of VLBI observations. Because it is empirical rather than theoretical, this model may contain contributions from sources other than ocean tides, such as the atmosphere.

3. Results and Discussion

As is well known, the retrograde diurnal motion of the pole is degenerate with long period nutation, and estimates of sub-daily polar motion can be contaminated by nutation model errors (see Eubanks [1993] for a lucid discussion). This is a result of retrograde diurnal polar motion being nearly fixed in Earth-centered inertial coordinates. Similarly, in our estimation strategies, mismodeled orbital variations in the GPS constellation that appear slow in an inertial frame can be readily absorbed by the retrograde diurnal component of polar motion. To avoid ambiguities from these error sources, we removed the retrograde diurnal band in our comparisons with VLBI data sets. (The VLBI polar motion data already have very little power at retrograde diurnal periods, owing to the explicit estimation of nutation corrections in the VLBI estimation strategy.) Furthermore, since we found that non-periodic signatures in our GPS polar motion series varied significantly with estimation strategy (and observed similar behavior among preliminary VLBI solutions), we restricted comparisons in this study to the semidiurnal (both prograde and retrograde) and diurnal prograde bands.

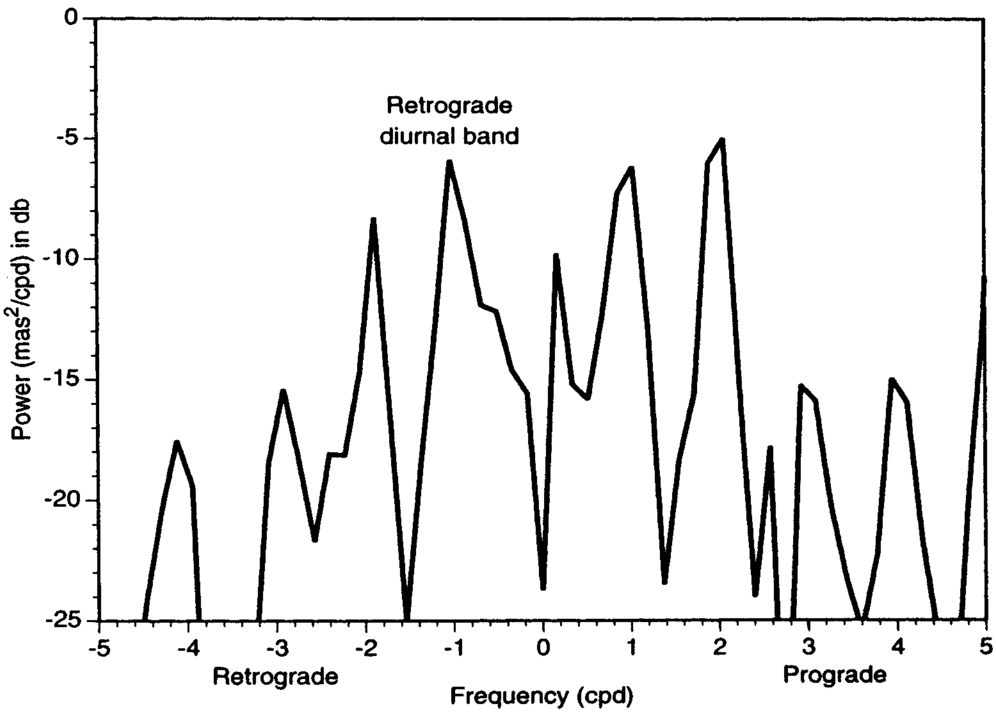

Fig. 1. GPS polar motion power spectral density.

In Figure 1, we show the power spectrum of the GPS polar motion series estimated every 30 minutes with loose (120 mas) constraints. As already mentioned, the GPS retrograde diurnal peak at –1 cycle/day (cpd) is contaminated by nutation and orbit mismodeling. The spectrum clearly shows peaks in the semidiurnal (±2 cpd) and prograde diurnal (+1 cpd) bands, with relatively little power elsewhere. The estimates are passed through a band reject filter so that only the +1 cpd and ±2 cpd bands, with bandwidths of 0.4 cpd, are retained. Identical filtering is applied to the VLBI series prior to comparison with the GPS data.

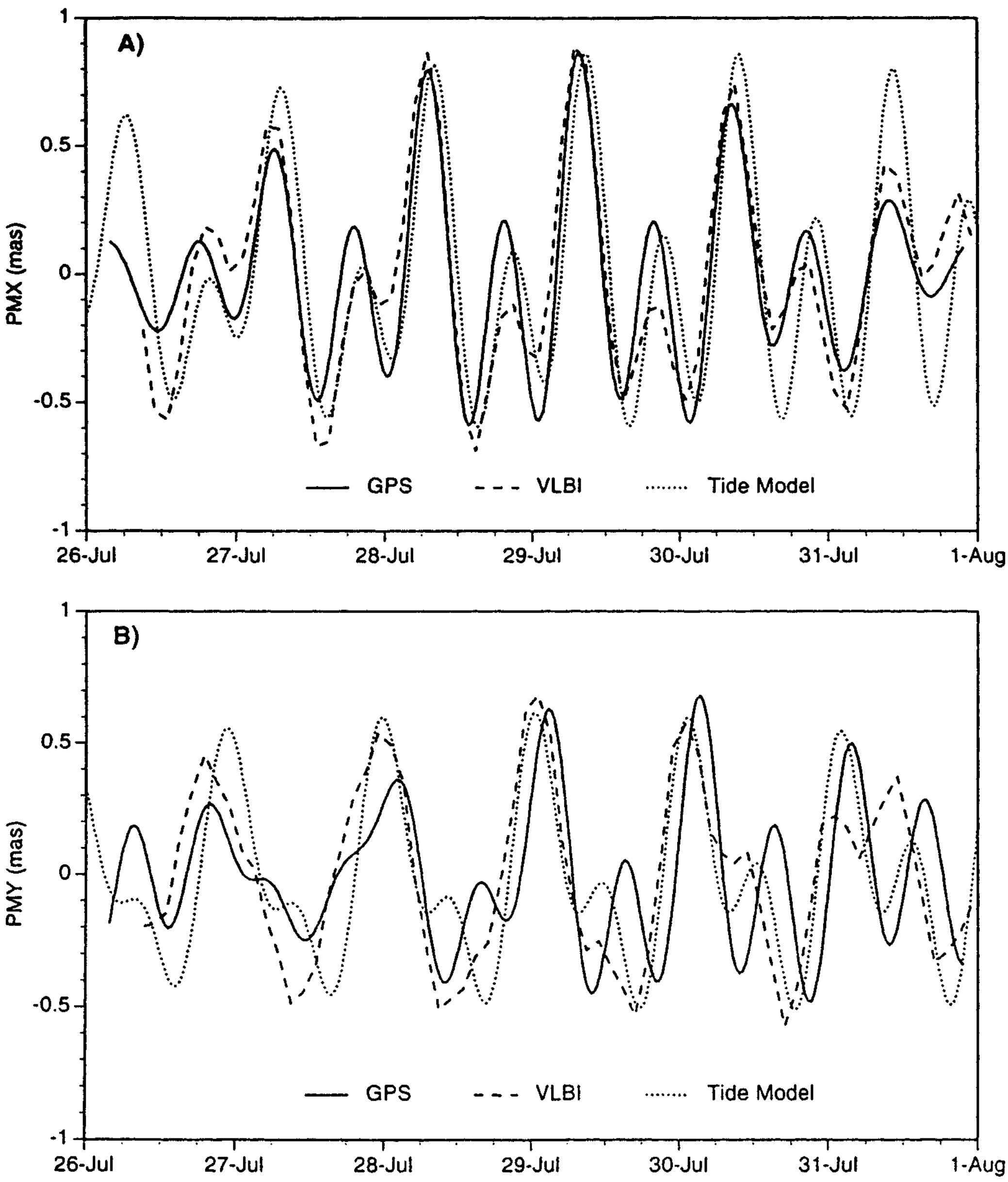

Fig. 2. (a) PMX semidiurnal and prograde diurnal bands for the GPS, VLBI, and Herring tide model time series. (b) Same as (a), but for PMY.

Figure 2 shows time-domain PMX and PMY plots of the diurnal (prograde) and semidiurnal (prograde and retrograde) bands of both the GPS and VLBI series, together with the Herring tide model. The rms difference between the VLBI and GPS series is 0.17 and 0.29 mas in PMX and PMY respectively. The overall level of agreement in both amplitude and phase is noteworthy, particularly in the x-component, and especially in light of the fact that the approximately 12-hour orbits of the GPS satellites might lead one to expect poor results at semidiurnal frequencies. Comparison statistics on rms differences and series cross-correlations are given in Table 1. The results in the table suggest that most of the GPS signal in Figure 2 can be attributed to ocean tides. The polar motion results presented here are very encouraging, and are consistent with similar good agreement between GPS and VLBI estimates of sub-daily UT1 variability [Freedman et al., 1993, and this volume]. We hope that this study will help in part to motivate future intensive VLBI campaigns to provide high-quality data for intercomparison with GPS.

Table 1. RMS Differences and Correlations

	x rms (mas)	y rms (mas)	x corr.	y corr.
VLBI - GPS	0.17	0.29	0.90	0.55
Tide Model - GPS	0.26	0.26	0.78	0.60
Tide Model - VLBI	0.25	0.26	0.80	0.77

ACKNOWLEDGMENTS. We are grateful to B. Haines, G. Hajj, L. Romans, J. Dickey, and R.. Muellerschoen for enlightening discussions. The work described in this paper was carried out in part by the Jet Propulsion Laboratory, California Institute of Technology, under contract with the National Aeronautics and Space Administration.

4. References

Boucher, C., Z. Altamimi, and L. Duhem, ITRF 91 and Its Associated Velocity Field, *IERS Technical Note 12*, Central Bureau of IERS, Observatoire de Paris, October 1992.

Blewitt, G., Advances in Global Positioning System Technology for Geodynamics Investigations: 1978-1992, in *Contributions of Space Geodesy to Geodynamics: Technology*, edited by D. E. Smith and D. L. Turcotte, pp. 195-213, Am. Geophys. Un., Washington, D.C., 1993.

Eubanks, T. M., Variations in the Orientation of the Earth, in *Contributions of Space Geodesy to Geodynamics: Earth Dynamics*, edited by D. E. Smith and D. L. Turcotte, pp. 1-54, Am. Geophys. Un., Washington, D.C., 1993.

Freedman, A. P., R. Ibanez-Meier, S. M. Lichten, J. O. Dickey, and T. A. Herring, Sub-Daily Earth Rotation During the EPOCH '92 Campaign, *Geophys. Res. Lett.*, submitted, 1993.

Gross, R. S., The Effect of Ocean Tides on the Earth's Rotation as Predicted by the Results of an Ocean Tide Model, *Geophys. Res. Lett.*, *20*, 293-296, 1993.

Herring, T. A., D. Dong, and R. W. King, Submilliarcsecond Determination of Pole Position using Global Positioning System Data, *Geophys. Res. Lett.*, *18*, 1893-1897, 1991.

Herring, T. A., and D. Dong, Measurement of Diurnal and Semidiurnal Rotation Variations and Tidal Parameters of the Earth, *J. Geophys. Res.*, submitted, 1993.

Lambeck, K. , *The Earth's Variable Rotation: Geophysical Causes and Consequences*, 449 pp., Cambridge University Press, New York, 1980.

Lichten, S. M., Toward GPS Orbit Accuracy of Tens of Centimeters, *Geophys. Res. Lett.*, *17*, 215-218, 1990a.

Lichten, S. M., Estimation and Filtering for High Precision GPS Positioning Applications, *Man. Geod.*, *15*, 159-176, 1990b.

Lindqwister, U. J., A. P. Freedman, and G. Blewitt, Daily Estimates of the Pole Position With the Global Positioning System, *Geophys. Res. Lett.*, *19*, 845-848, 1992.

McCarthy, D. D. (ed.), IERS Standards, *IERS Technical Note 3*, Central Bureau of IERS, Observatoire de Paris, 1992.

Seiler, U., Periodic Changes of the Angular Momentum Budget Due to the Tides of the World Ocean, *J. Geophys. Res.* , *96*, 10287-10300, 1991.

Wunsch, J., and U. Seiler, Theoretical Amplitudes and Phases of the Periodic Polar Motion Terms Caused by Ocean Tides, *Astron. Astrophys.*, *266*, 581-587, 1992.

DIURNAL AND SEMIDIURNAL VARIATIONS IN EARTH ORIENTATION DETERMINED FROM LAGEOS LASER RANGING AND GPS

MICHAEL M. WATKINS, RICHARD J. EANES,
AND JOHN G. SONNTAG
The University of Texas at Austin
Center for Space Research 60605
Austin, TX 78712 U.S.A.

ABSTRACT. Two analyses of high frequency Earth orientation were performed. In the first study, variations in universal time and polar motion due to ocean tides at nearly diurnal and nearly semidiurnal frequencies were determined from analysis of laser ranging to the Lageos satellite over the period from 1987 to 1992. The adjusted diurnal tides were K_1, S_1, P_1, O_1 and Q_1, while the semidiurnal tides were K_2, S_2, M_2, and N_2. In the second study, daily estimates of diurnal and semidiurnal UT1 variations were determined for a 49-day interval during the summer 1992 IGS campaign using doubly differenced GPS phase data. The results were then compared to the tidal variations observed from Lageos. For both studies, formulations were used that explicitly separated prograde and retrograde terms in the polar motion in order to eliminate aliasing from the singularity of retrograde wobble with long period orbit error and nutation. The results of the EOP variations at tidal frequencies obtained in this study agree well with those from the VLBI studies, typically at the 2–3 μs level in universal time and 30–50 μas level in polar motion. The results from the GPS analysis indicated independent daily determination of diurnal and semidiurnal variations of UT1 with accuracies at the 20–30 μs level.

1. Procedure

The solution for the tidal variations, described in detail in Watkins and Eanes [1993], was performed using the exact alias frequency of the tides in question as shown below, and adjusting a single amplitude and phase for each tidal frequency.

$$m = \sum_{s=1}^{N} [m_p^{s+} \exp(i\,\theta_s) + m_p^{s-} \exp(-i\,\theta_s)] = x - iy$$

where θ_s is the instantaneous phase of the particular tide in question, and m_p^{s+} and m_p^{s-} are complex prograde and retrograde subdiurnal polar motions modulated by the tidal frequency. We define the real and imaginary parts of m_p^{s+} and m_p^{s-} in terms of the usual x_p and y_p components as:

$$m_p^{s+} = x_p^{s+} - iy_p^{s+}$$

$$m_p^{s-} = x_p^{s-} - iy_p^{s-}$$

where x_p^{s+}, x_p^{s-}, y_p^{s+}, and y_p^{s-} were the real variables estimated using the SLR data. The singularity between retrograde nearly diurnal polar motion and the satellite orbit is avoided by removal (nonestimation) of the retrograde quantities for diurnal tides.

High frequency variations in UT were modeled as.

$$\delta \mathrm{UT1} = \sum_{s=1}^{N} [u^{sc} \cos(\theta_s) + u^{ss} \sin(\theta_s)]$$

where u^{sc} and u^{ss} were the real parameters estimated. For both wobble and UT1, the index s varied over 9 total ocean tide frequencies listed above. The preliminary solution described above was performed using 6 years of Lageos data spanning the period 1987–1992, the period of highest quality Lageos data. Approximately 400,000 two-minute normal points from 70 tracking sites formed this data set. The models used in the data analysis adhered generally to the IERS standards with several notable exceptions. The static geopotential model was JGM-1, and changes in the geopotential due to ocean tides were modelled using an enhanced model which included all terms, chosen from a degree and order 20 spherical harmonic expansion, with perturbations that exceeded 1 mm in either the radial, normal, or transverse components of the orbit, respectively. The nominal coefficients were from the model of Schwiderski [1980], with a subset of terms adjusted at the UTCSR from a multisatellite solution. The perturbations were determined from an analytic approach due to Casotto [1989]. The tidal amplitudes at frequencies not included in the original Schwiderski model were extrapolated using an assumption of admittances which vary linearly with frequency.

The solid tide model was expanded to include geopotential variations due to third degree terms, assuming the Love number, k_3 of 0.093 [Wahr, 1981]. Finally, the free core nutation period was changed from 460 to 430 days.

The reference frame was fixed to the CSR93L01 system of Eanes and Watkins [1993] which was determined from analyses of the entire Lageos mission, adjusting positions for over 110 sites and horizontal velocities for 47 sites. Sites with unadjusted velocities were assumed to have the velocities predicted by the NUVEL-1NNR model of Argus and Gordon [1991]. Site-dependent nuisance parameters such as range or clock biases were adjusted where necessary.

In the estimation process, mean orbital elements (excluding the nodal longitude), x_p, y_p, and UT1 were adjusted every 3 days, along with the diurnal and semidiurnal prograde and retrograde wobbles and UT1 variations. Using the above modelling and parametrization, the postfit range residual rms was 22 millimeters. The results of the adjustment are presented in the following table, along with conservative estimates of the uncertainties. The uncertainties included in the table are scaled formal uncertainties. The scale factor has been derived through comparison of Earth orientation and site positions with external solutions, such as those derived from VLBI, in order to make the formal uncertainties consistent with the inferred accuracy. Error analyses described in Watkins and Eanes [1993] support these uncertainties.

For the second study, the analysis of 49 days of GPS data, variations in universal time at exactly once and twice per sidereal day were adjusted for each day, along with initial conditions for each

Observed Tidal Variations in UT1 and Polar Motion

Tide	X_p^+, μas	Y_p^+, μas	X_p^-, μas	Y_p^-, μas	$UT1_c$, μs	$UT1_s$, μs
K_1	158±30	5±30	–	–	4.8±3	14.7±3
K_1^*	–	–	–	–	5.7±3	13.1±3
S_1	−51±30	−38±30	–	–	1.3±3	4.4±3
P_1	−25±30	19±30	–	–	−2.0±3	−1.1±3
Q_1	−41±20	−5±20	–	–	−4.0±2	−7.9±2
O_1	−131±20	9±20	–	–	−20.8±2	−17.3±2
O_1^*	–	–	–	–	−17.0±2	17.2±2
K_2	0±20	−23±20	20±30	−5±30	1.4±3	0.6±3
S_2	7±20	−81±20	−56±30	127±30	3.0±3	7.8±3
M_2	51±20	−114±20	25±20	195±20	−7.6±2	15.1±2
N_2	2±20	−21±20	2±20	18±20	−2.8±2	3.8±2

* corrected for 18.6-year sideband effects

GPS satellite, site dependent zenith delays every 2.5 hours, and phase ambiguities where necessary. The model for EOP variations was:

$$\delta \mathrm{UT1} = \sum_{n=1}^{N} [u^{nc} \cos(n\,\theta_g) + u^{ns} \sin(n\,\theta_g)]$$

where θ_g is the Greenwich sidereal time, and u^{nc} and u^{ns} are the real parameters estimated with the GPS data. The models used in the analysis generally adhered to the IERS Standards or appropriate International GPS Service recommendations, as above, with the exception of the use of the University of Texas TEG-2 gravity field.

In order to compare these results to the EOP variations at the tidal frequencies derived above, we reconstructed the equivalent variations at exactly once and twice per sidereal day from the sum of the 5 diurnal and 4 semidiurnal tides, respectively. These variations were then compared with the variations observed with GPS. The results, discussed in Sonntag and Watkins [1993], indicated 20 to 30 microsecond agreement between the two series, with slightly better agreement for the semidiurnal terms. The formal uncertainties on the daily GPS estimates were on the order of 15 to 20 microseconds.

2. References

Argus, D.F. and Gordon R.G. (1991) No-net-rotation model of current plate velocities incorporating plate motion model NUVEL-1, *Geophys. Res. Lett., 18*, 2039–2042.

Casotto, S. (1989) Ocean tide models for TOPEX precise orbit determination, Ph.D. dissertation, Univ. of Tex. at Austin.

Eanes, R.J. and Watkins, M.M. (1993) The Center for Space Research Solution CSR93L01, submitted to the International Earth Rotation Service.

Schwiderski, E.W. (1980) Ocean tides. Part I: Global ocean tidal equations, *Marine Geod.*, *3*, 161–216.

Sonntag, J.G. and Watkins, M.M. (1993) Measurement of subdiurnal variations in UT1 using the Global Positioning System, submitted to *Geophys. Res. Lett.*

Wahr, J.M. (1981) Body tides on an elliptical, rotating, and oceanless Earth, *Geophys. J. R. Astron. Soc.*, *64*, 677.

Watkins, M.M. and Eanes, R.J. (1993) Diurnal and semidiurnal variations in Earth orientation determined from Lageos laser ranging, submitted to *J. Geophys. Res.*

HIGH FREQUENCY FLUCTUATIONS OF POLAR MOTION DURING IGS'92 CAMPAIGN

Huang Chengli[1], Jing Wenjin[1], Liao Dechun[1], Zhu Wenyao[1], Wang Jiexian[2]
[1] *Shanghai Observatory, Chinese Academy of Sciences, 80 Nandan Road, Shanghai 200030, P.R.China*
[2] *Tongji University, Shanghai 200092, P.R.China*

ABSTRACT. During IGS'92 Campaign seven PM(Polar Motion) series provided by GPS Processing Centers are analysed in this paper. Some similar high frequency fluctuations in these PM series are detected by using spectral analyses, least square adjustment and F-test as follows: there are short periodic fluctuations of 27.0, 16.5, 13.4, 10.4 day in X direction; and of 10.0, 20.5, 15.8 day in Y direction. And there are similar systematic deviations derived from the comparison of each series with EOP(IERS) 92 C 04. The main cause of these systematic deviations is that the rotation between the reference frames of these series and ITRF91 exists. As for the reason, the coordinates of stations are not fixed (or partly fixed only) when solving X and Y with GPS data. The high frequency fluctuations of polar motion are explained to some extent by the excitation of atmospheric angular momentum.

1. Introduction

With the improvement of GPS observational precision and the increase of the observations, especially due to its convenience and cheapness, GPS has become an important technique for geodesy and geodynamics. GPS Coordinating Centre was set up by IERS at 1989. Some scientific results have been attained from the GIG'91 Campaign (Jan.22- Feb.13,1991) which is the first attempt at coordinating on an international basis and is the efforts of a number of participants in deploying a globally distributed network of GPS tracking stations[1]. IGS'92 Campaign completed its scientific task during Jun.21-Sep.22,1992. More than six hundred stations took part in EPOCH'92 (Jul.26-Aug.8) in which VLBI, SLR and LLR were also adopted in order to campare various techniques. Shanghai Observatory(China) attended this Campaign, and has processed global GPS data. There is now a total of eight GPS analysis centers contributing on a regular basis their EOP(Earth Orientation Parameters) and TRF(Terrestrial Reference Frame)results to the IERS Central Bureau and sub-Bureau for rapid service and predictions. During IGS'92 Campaign, some polar motion series accumulated by these centers are analysed and compared in this paper.

2. Materials and data used

Six polar motion series[2] discussed in this paper are obtained from IGS'92 Earth Orientation Bulletin (Table 1).

Table 1. Materials and data used

No.	Series	Interval
1	EOP(CSR) 92 P 01	27 Jun. - 5 Sep. 1992
2	EOP(CODE) 92 P 04	27 Jun. - 5 Sep. 1992
3	EOP(JPL) 92 P 02	27 Jun. - 5 Sep. 1992
4	EOP(SIO) 92 P 03	27 Jun. - 5 Sep. 1992
5	EOP(ESOC) 92 P 01	27 Jun. - 5 Sep. 1992
6*	EOP(GFZ) 92 P 01,02	27 Jun. - 5 Sep. 1992
7	EOP(SHA) 92 P 01	24 Jul. - 10 Aug. 1992
8**	EOP(COM.) 92 P 01	27 Jun. - 5 Sep. 1992

* Because EOP(GFZ) 92 P 01,02 is not in the same series, we do not use this series for the following analyses.

A new combined EOP(COM.) 92 P 01 series marked on " * *" at above table is obtained from series No.1,2,3,4,5 in order to compare with AAM instead of each series in section 5 this paper. For this series the weight is considered as follow:

$$p_{ij} = (e_i^{-2} / \sum_{i=1}^{5} e_i^{-2}) \cdot (u_{ij}^{-2} / \sum_{j=1}^{n_i} u_{ij}^{-2})$$

So

$$r_{cj} = \sum_{i=1}^{5} r_{ij} \cdot p_{ij} / \sum_{i=1}^{5} p_{ij}$$

where for ith series

e_i	estimated uncertainty (from Tab.4 cited in [3])
r_{ij}	value of X,Y at epoch j
u_{ij}	observational error
r_{cj}	combined value of X,Y at epoch j
n_i	number of observational data of the ith series

In 1992, a software SHAGAP was developed in Shanghai Observatory. Using this program, the global GPS observational data during EPOCH'92 were processed and many scientific results were obtained. The series of polar motion EOP(SHA) 92 P 01[4] is one result.

3. High frequency fluctuations and systematic deviations of polar motion

3.1. METHODS

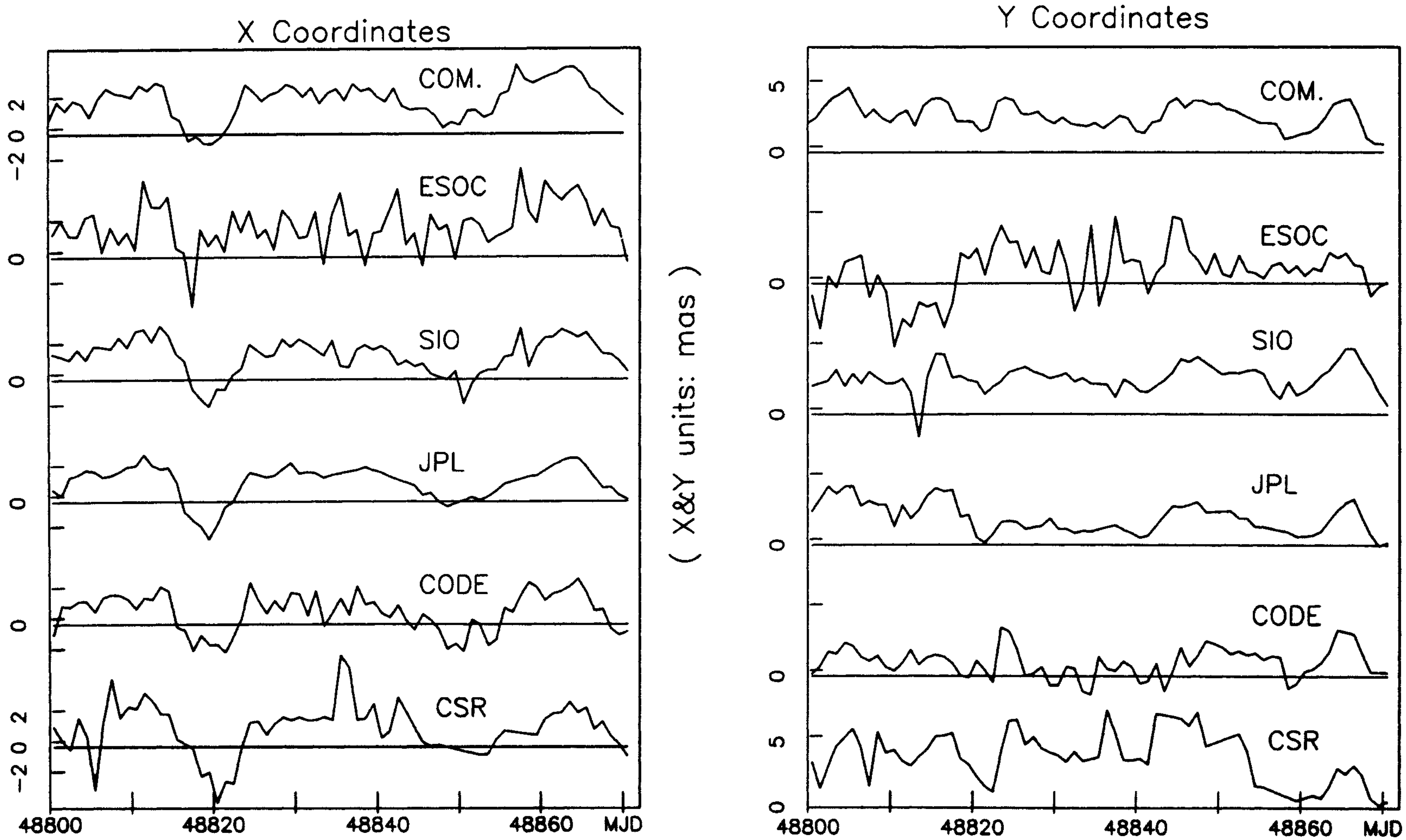

Fig.1 High-pass-filtered Polar Motion

Fig.2 Spectra of Polar Motion

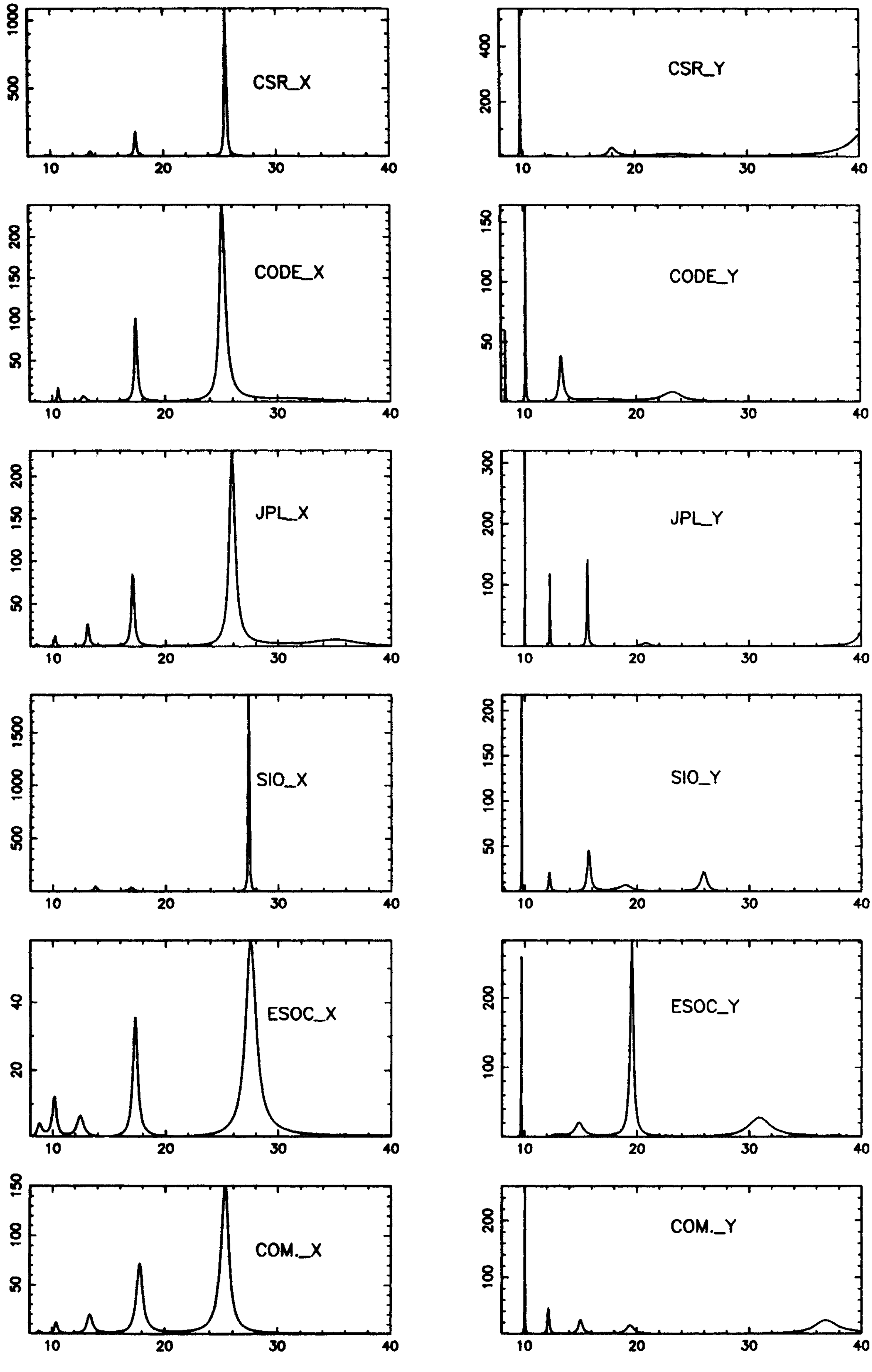

In order to analyse the high frequency variations of X and Y, it is necessary that the part of low frequency of above series should be removed and the parts of high frequency were reserved. Firstly, the part of low frequency (longer than 35 day) for EOP(IERS) 90 C 04 is obtained by using Vondrak low-pass-filter (filter factor ϵ =3.d-5). Secondly, the parts of high frequency (sub-35 day) of above series are derived after reduction of the part of low frequency of EOP(IERS) 90 C 04 from each series (Fig.1). Finally, the spectra of each series (Fig.2) were processed by maximum entropy method, and simultaneously, some periodic fluctuations P_i(day), amplitude Am_i(mas) and bias a(mas) of each series (Table 2) are fitted by least square adjustment and tested by F-test, where the bias a is the systematic deviation between each series and IERS. Because the interval of EOP(SHA) 92 P 01 is too short (18 day only) to make spectral analyses, the systematic deviation a is obtained only.

Table 2 : High frequency fluctuations and systematic deviations

	Series	a^* (mas)	P_1 (day)	Am_1 (mas)	P_2 (day)	Am_2 (mas)	P_3 (day)	Am_3 (mas)	P_4 (day)	Am_4 (mas)
X	CSR	1.2	27.5	1.3 ± 0.3	16.4	0.9 ± 0.3	13.0	0.8 ± 0.3	9.4	0.4 ± 0.2
	CODE	0.8	27.4	1.3 ± 0.2	16.8	0.7 ± 0.2	12.3	0.4 ± 0.2	10.2	0.3 ± 0.2
	JPL	1.3	28.7	1.2 ± 0.1	17.3	0.5 ± 0.1	12.5	0.5 ± 0.1	/	/
	SIO	1.5	27.2	1.3 ± 0.1	16.0	0.6 ± 0.1	12.8	0.5 ± 0.1	/	/
	ESOC	2.0	27.2	0.8 ± 0.2	16.5	0.8 ± 0.2	/	/	10.4	0.4 ± 0.2
	COM.	2.1	26.9	1.2 ± 0.2	16.2	0.7 ± 0.1	13.4	0.4 ± 0.1	10.4	0.3 ± 0.2
	SHA	5.7								
Y	CSR	3.8	10.0	1.1 ± 0.3	20.6	0.6 ± 0.3	22.8	0.6 ± 0.3		
	CODE	1.0	10.0	0.8 ± 0.2	20.5	0.5 ± 0.2	13.8	0.7 ± 0.2		
	JPL	2.1	9.9	0.9 ± 0.2	/	/	15.9	0.5 ± 0.2		
	SIO	2.7	9.7	0.9 ± 0.2	19.2	0.4 ± 0.2	15.8	0.5 ± 0.2		
	ESOC	0.9	9.9	0.6 ± 0.3	20.0	0.9 ± 0.3	/	/		
	COM.	2.7	10.0	0.7 ± 0.2	20.5	0.5 ± 0.2	15.3	0.4 ± 0.2		
	SHA	3.5								

* a is systematic deviation

3.2. RESULTS

As shown in Fig.2 and Table 2, similar fluctuations exist in the above series. In X direction, there are fluctuations with periods of 27.0, 16.5, 13.4 and 10.4 day and its maximum amplitude is 1.2mas (27.0day). In Y direction, there are of 10.0, 20.5, 15.8 day, the maximum amplitude is 0.9mas (10.0day). And there are also systematic deviations for combined series. They are about 2.1mas(X) and 2.7 mas(Y).

4. Systematic deviation and reference frame

In processing GPS data, in order to set up a reference frame, it is usual to fix the coordinates of some stations (theoretically more than three) with high precision as fiducial stations which are not considered in the adjustment. But there are two problems. One is that there are no or few stations satisfying the demand of precision of fiducial station[5] (i.e. better than 2 cm). For example, when GPS data observed during EPOCH'92 Campaign are processed in Shanghai Observatory, the criterion of fiducial station is the priori error of station coordinates smaller than 2 cm. As a result, there are about twenty coordinates (no height) fixed, and they are mostly coordinates of American sites. The other problem is that the selected fiducial stations may altogether locate at one region (i.e. American or European). That is to say, they may not be well-distributed globally. And even if there are a few fiducial stations meeting the need, from the point of view of the effect to fix reference frame, these stations are of little use. The direct result of these two problems is that the reference frame is not perfectly fixed as need (i.e. fixed at ITRF91), it has a rotation relative to ITRF, so the solved station coordinates and polar coordinates have a rotation too. As a result, the rotation induces the systematic deviations between various series and IERS as mentioned above.

For example, EOP(SHA) 92 P 01 is taken to study the relation between its reference frame (named TRF(SHA)) and ITRF91.

Among the twenty-four stations of TRF(SHA), just seven station coordinates are given directly in Table T-3 cited in [1] in which station coordinates in the ITRF91 are listed, and similarly, there are twenty-one stations are listed in ITRF92 Table T-3 cited in [6]. And noted that there is not rotation between ITRF91 and ITRF92[6], so ITRF92 are used to compare with TRF(SHA) instead of ITRF91. These twenty-one stations are well-distributed globally, they are: ALBH, ALGO, DRAO, DS10, DS60, FAIR, GRAZ, HART, JPL1, KOSG, MASP, METS, ONSA, PAMA, PIN1, SANT, STJO, TAIW, USUD, YAR1 and YELL.

$\vec{r}_{SHA}$ is the average position during EPOCH'92 at epoch MJD48835.5, so the coordinates of the twenty-one stations of ITRF92 should be transferred from epoch 1988.0 (MJD47160) to MJD48835.5. Here the plate motion is considered only and the equation for this transfer will be as follows:

$$\vec{r}_{IERS} = \vec{r'}_{IERS} + \vec{V} \cdot (t - t_0)$$

so observational equation is

$$\vec{r}_{SHA} = \vec{r}_{IERS} + \vec{t} + \Theta \vec{r}_{IERS} + \vec{e}$$

where

$$\vec{t} = (t_1, t_2, t_3)^T$$

$$\Theta = \begin{pmatrix} D & -R_3 & R_2 \\ R_3 & D & -R_1 \\ -R_2 & R_1 & D \end{pmatrix}$$

$$\vec{e} = \text{accidental error}$$

equation can also written as

$$\vec{L}_{63\times1} = \Theta_{63\times7}\vec{X}_{7\times1} + \vec{e}_{63\times1}$$

the least square solution will be

$$\vec{X} = (\Theta^T \vec{P} \Theta)^{-1} \Theta^T \vec{P} \vec{L}$$

where weight $\vec{P}$ are calculated from the precision of $\vec{r}_{SHA}$

$$p_i = \sigma_i^{-2} / \sum_{i=1}^{n} \sigma_i^{-2}$$

thus, the transfer parameters from TRF(SHA) to ITRF92 are solved:

$$t_1 = -18.4 \pm 1.7cm$$
$$t_2 = -13.3 \pm 1.8cm$$
$$t_3 = 2.7 \pm 1.5cm$$
$$D = (-1.08 \pm 0.22) * 10^{-8}$$
$$R_1 = 2.67 \pm 0.75mas$$
$$R_2 = 5.14 \pm 0.63mas$$
$$R_3 = 8.87 \pm 0.52mas$$

Using these transfer parameters, polar coordinates of EOP(SHA) 92 P 01 are transfered from TRF(SHA) to ITRF92, then, the average difference between them and the polar coordinates of IERS in eighteen days are obtained, they are about 4.92mas (X) and 3.46mas (Y). And they correspond to the solution derived in section 2 ($\Delta X_p = 5.7mas, \Delta Y_p = 3.5mas$).

These results have shown that the systematic deviations of series are mainly induced by the rotation of terrestrial reference frames of series which are not completely fixed on ITRF91(or ITRF92) during the processing of GPS data.

So, it is recommended that it should have more and globally well-distributed stations possibly fixed at ITRF91 or ITRF92 when X and Y are solved, or the rotation parameters be given and the influence of them be considered.

5. High frequency fluctuation in X and Y and the excitation of Atmospheric Angular Momentum(AAM)

The correlation between the variation of earth rotation and the atmospheric excitation has been studied by many authors[7], who explained well that the variations of Length Of Day(LOD) from irregular short periodic (40-50 day) to years are caused by the exchange of angular momentum between the Earth and atmosphere, and the sub-daily variation of LOD is due to ocean and tide[8][9]. But the explanation of variation of polar motion caused by atmosphere is not as good as that in LOD.

Taking EOP(COM.) 92 P 01 as an example, the correlation between the polar motion during IGS'92 Campaign and the AAM-induced polar motion is studied in this section.

The atmospheric data are from NMC(USA) and JMA(Japan). In NMC, the data of effective excitation functions $\vec{\chi}(\chi_1, \chi_2, \chi_3)$ cover whole year of 1992 and are given at two points each day. There are wind component in southern and northern hemisphere χ^{sw}, χ^{nw} (limit to 50 mb and to 100mb) and pressure component χ^{sp}, χ^{np} (No Inverter-Barometer(N.I.B.) and With I.B.(W.I.B.)). In JMA $\vec{\chi}$ data have four points each day during Jun.21-Sep.30,1992 and there are wind component χ^{w} and pressure component χ^{p}(N.I.B. and W.I.B.). Then effective excitation functions are expressed as the following formulum:

$$\vec{\chi} = \chi^{sw} + \chi^{nw} + \chi^{sp} + \chi^{np}$$

In this paper, wind component is limited to 50 mb, and pressure component(W.I.B.) is used. PM reduced by $\vec{\chi}$ is[10]:

$$\vec{m}(t) = e^{i\sigma t}[\vec{m}(0) - i\sigma(1 + \sigma/\Omega)\int_0^t \vec{\chi}(\tau)e^{-i\sigma\tau}d\tau] - (\sigma/\Omega)[\vec{\chi}(t) - e^{-i\sigma t}\vec{\chi}(0)]$$

where,$\sigma = 2\pi/435day^{-1}$, the mean rotation rate of the solid earth $\Omega = 7.29 \times 10^{-5}s^{-1}$

$\vec{m}(t)$ depends on initial value $\vec{m}(0)$, but $\vec{m}(t)$ will rapidly tend to be stable after calculation several times repeatedly. In this paper, $\vec{m}(0)$ is adopted from EOP(IERS) 90 C 04. And using one-degree integration approach:

$$\int_0^t f d\tau = \frac{1}{2}(f + f')t$$

In order to compare with the high frequency fluctuation of PM of EOP(COM.) 92 P 01, it is necessary to filter $\vec{m}$ induced from atmospheric data of NMC and JMA as done in section 3.1 for keeping the fluctuation of sub-35 day (ϵ = 3.d-5, Fig.3). In plot, the X and Y coordinates of EOP(COM.) 92 P 01 move downwards with a constant i.e. their systematic deviations:

$$X = x - 2.1mas$$

$$Y = y - 2.7mas$$

As shown in Fig.3, there are some similar trends between X and m1, but it does not happen between Y and m2.

In Table 3 the correlation coefficients between PM of EOP(COM.) 92 P 01 and AAM-induced PM of two meterological centers, JMA and NMC are given.

Table 3 Correlation between GPS-observed and AAM-induced Polar Motion

	NMC	JMA
X	0.70	0.81
Y	0.10	0.21

From Fig.3 and Table 3, some results can be obtained:
(1) The amplitudes of X and Y are larger than those of m1,m2, and the high frequency variation in X can be explained partly as the results of excitation of AAM;
(2) Due to the growth in number of observations and the improvement of the observational precision during EPOCH'92 (MJD48828-48840), X and Y are well consistent with m1,m2;
(3) The systematic deviations of X and Y are confirmed again.

6. Summary

Fig.3 Polar Motion of high frequency

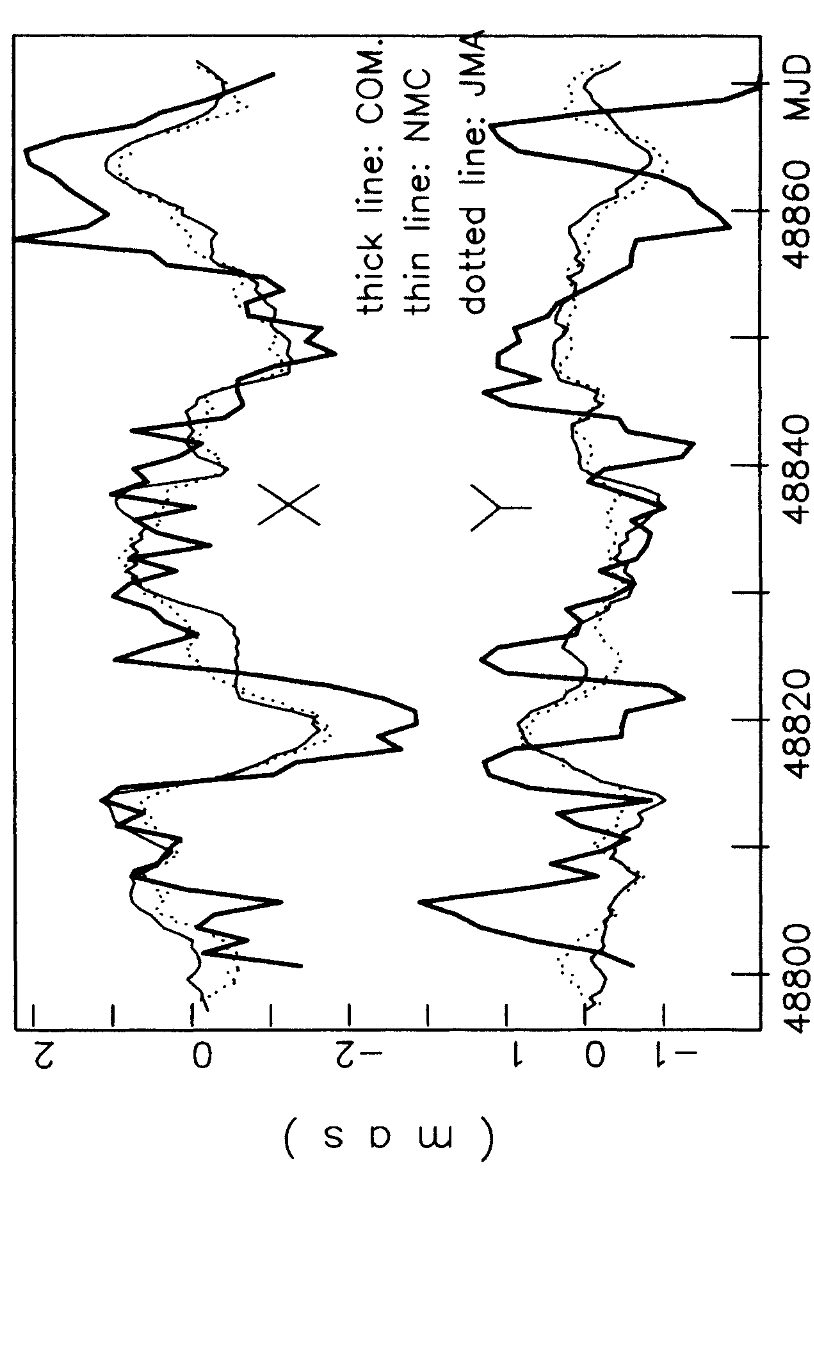

(1) There are similar high frequency fluctuations among the series of Polar Motion during IGS'92 Campaign. In X direction, the fluctuations have periods of 27.0, 16.5, 13.4, 10.4 day, of which the maximum amplitude is 1.2 mas(27.0day), and in Y direction, the fluctuations are of 10.0, 20.5, 15.8 day, of which maximum amplitude is 0.9 mas(10.0day).

(2) There are also systematic deviations with the same sign between above series and EOP(IERS)92 C 04. which values are about 2.1 mas in X and about 2.7 mas in Y while they are 5.7 mas in X and 3.5 mas in Y reduced in Shanghai Observatory. The main reason of these systematic deviations is that there is rotation between the reference frame of these series and ITRF91 (or ITRF92). The station coordinats are not fixed (or are partly fixed only) when solving X and Y with GPS data so the rotation exists.

(3) The high frequency fluctuations of polar motion can be explained partly as the result of excitation of atmospheric angular momentum. And the systematic deviations are confirmed again.

Acknowledgement We thank IERS for disturbuting the EOP series from six analysis centers, thanks to Dr. Richard S. Gross and David A. Salstein for their kindness to offer us the atmosphere data of JMA and NMC, and special thanks are due to Professor Dawei Zheng for his help on many details.

Reference

[1] 1991 IERS Annual Report, pp.IV-15, pp.II-38

[2] Huang,C.L., et al., 1993, High frequency fluctuations of X and Y polar coordinates derived from various GPS analysis centers, IAG General Meeting, Beijing, 1993

[3] IGS'92 Campaign: Comparisons of GPS, SLR and VLBI, Earth Orientation Determinations (Final Report), 1992

[4] Wang,J.X., 1993, The application of GPS to Geodesy and Geodynamics (in Chinese, Dr. thesis)

[5] IGS'92 Campaign: Comparisons of GPS, SLR and VLBI, Earth Orientation Determinations (First Report), 1992

[6] 1992 IERS Annual Report, pp.II-46, pp.II-38

[7] Lambeck,K., 1980, The Earth's variable rotation: geophysics causes and consequences, Cambridge University Press, pp.449

[8] Hide,I.N., et al. 1980, Nature, Lond., 286, pp.114-117

[9] Langley,R.B., et al. 1981, Nature, Lond., 294, pp.730-732

[10] Barnes,R.T.H., et al. 1983, Proc. R. Soc. Lond., A387, pp.57

SHORT - TERM POLAR MOTION AND UT1 VARIATIONS OBSERVED BY IGS

Jan Hefty*

The GPS polar motion and UT1 series available from the IGS'92 Campaign and its continuation are compared with the geodetic IERS combined series and the modelled atmospheric series based on effective atmospheric angular momentum functions. The short-term oscillations are obtained by removing the long periodical variations of the individual series. Polar motion variations in range from days to months are observed by GPS and significant correlation with both IERS combined and atmospheric series is found. The correlation of GPS UT1R with geodetic combined and atmospheric series reaches maximum for weekly variations. The monthly GPS UT1 oscillations exhibit discrepancies with other series.

ANALYZED DATA

The daily GPS series from 3 processing centers CODE, JPL and SIO are available for almost whole period 1992.5-1993.0. They give polar motion and the CODE series also UT1. The daily IERS series based on combination of VLBI, SLR and LLR observations [1] gives x, y, UT1 and covers the whole IGS Campaign. For the UT comparisons we use also the daily VLBI series from Westford - Wettzell baseline. The complete Yoder et. al [2] model for periodic variations due to zonal tides is removed from all UT1 series. In Table 1 we summarize the data used in further comparison studies.

The EOP variations caused by meteorological excitations have been obtained from time series of atmospheric angular momentum χ-functions at 12-hour intervals computed from pressure and wind fields generated at the Japan Meteorological Agency [3]. The motions of Celestial Ephemeris Pole $\mathbf{p}(t)=p_1+ip_2$ induced by atmospheric fluctuations $\chi=\chi_1+i\chi_2$ are computed from linearized Liouville equation [4]

* Observatory of the Slovak Technical University, Department of Theoretical Geodesy, Radlinskeho 11, 81368 Bratislava, Slovak Republic

$$\mathbf{p}(t)+\frac{i}{\sigma_0}\frac{d\mathbf{p}(t)}{dt}=\boldsymbol{\chi}(t) \quad , \tag{1}$$

where σ_0 is frequency of Chandler wobble. Let $\mathbf{P}(\omega)$ denote the Fourier transform of $\mathbf{p}(t)$ and $\mathbf{X}(\omega)$ the Fourier transform of $\boldsymbol{\chi}(t)$. Then eq.(1) transformed into frequency domain becomes

$$\mathbf{P}(\omega)=\frac{\sigma}{\sigma-\omega}\mathbf{X}(\omega) \quad . \tag{2}$$

The procedure used to compute the AAM induced polar motion consist in Fast Fourier Transform (FFT) of $\boldsymbol{\chi}(t)$, multiplication with transfer function (2) and recovering $\mathbf{p}(t)$ by inverse FFT. Two alternatives of $\mathbf{p}(t)$ from χ-functions have been obtained according to the pressure term used - with and without the inverted barometer (IB) approximation.

The atmosphere induced UT is inferred from χ_3 component (wind term and pressure term with IB) by numerical integration.

Table 1
Analyzed series

Technique	Series	Period	EOP
GPS	EOP(CODE) 92 P 04	1992 Jun. 19 - 1993 Jan. 26	x,y,UT1
GPS	EOP(JPL) 92 P 02 EOP(JPL) 92 P 03	1992 Jul. 17 - 1992 Nov. 14 1992 Nov. 15 - 1993 Jan. 16	x,y
GPS	EOP(SIO) 92 P 03	1992 Jun. 7 - 1993 Nov. 12	x,y
Combined	EOP(IERS) 90 C 04	1992 Jan. 1 - 1993 Jan. 31	x,y,UT1
VLBI	EOP(NOAA) 92 R 02	1992 Jan. 1 - 1992 Dec. 31	UT1
AAM	AAM(JMA) 92 * 01	1992 Jan. 1 - 1992 Dec. 31	χ_1,χ_2,χ_3 -> x,y,UT

HIGH FREQUENCY VARIATIONS OF EARTH ROTATION PARAMETERS

The short-term oscillations of x, y and UT1R as well as of the AAM induced series are obtained by removing the long periodical variations of the individual series. Three types of residuals according to degree of Vondrak [5] smoothing are analysed. Fig.1 shows transfer functions of the used filters. The cut-off periods 9 days (filter I), 30 days (filter II) and 90 days (filter III) correspond roughly to daily, weekly and monthly variations of residuals.

Fig.2 and Fig.3 show the high pass filtered monthly and daily oscillations of the three GPS polar motion solutions and the AAM induced polar motion based on JMA pressure term without IB approximation for the period 1992.5-1993.0. Mean formal uncertainties of GPS series are 0.11 mas for CODE, 0.18 mas for JPL and 0.20 mas for SIO. The upper graphs show that the individual GPS series follow the same pattern which is sporadically identical with AAM variations. The daily variations in lower graphs have significantly larger scatter for CODE and SIO series when compared with JPL polar motion and significantly exceed the formal uncertainties.

Fig.4 shows the UT1R residuals of GPS CODE series, combined IERS series as well as the UT AAM series. The monthly GPS variations differ from IERS and AAM in the beginning of IGS campaign, the daily variations of the three series have similar behaviour.

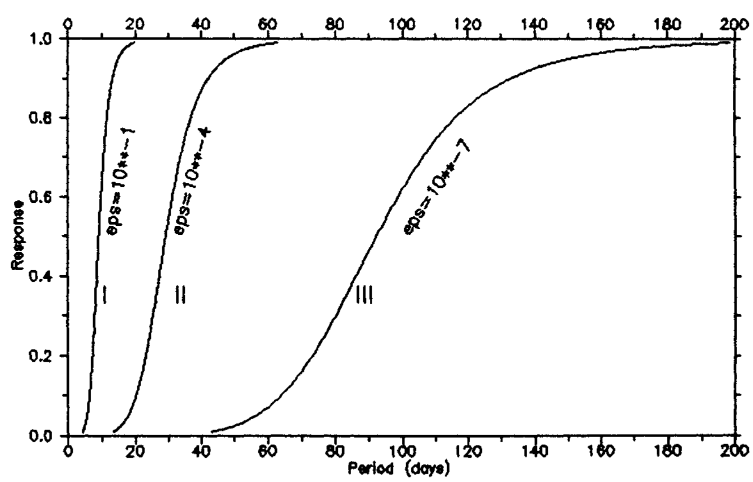

Fig.1 Transfer functions of Vondrak smoothing

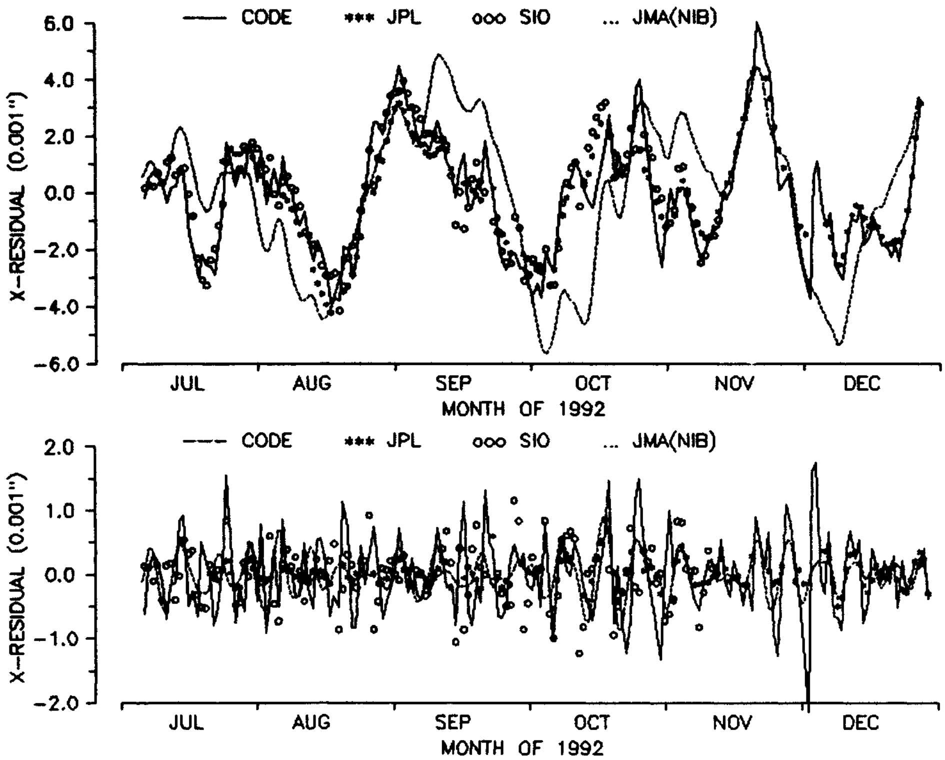

Fig.2 x-coordinate residuals from smoothing III (upper graph) and from smoothing I (lower graph)

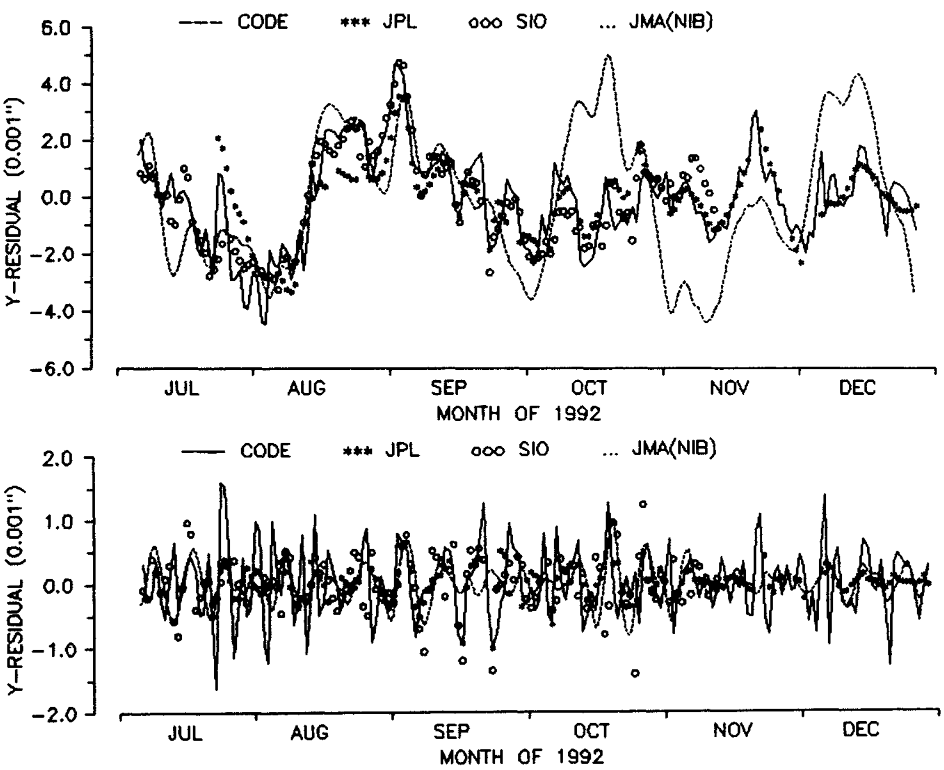

Fig.3 y-coordinate residuals from smoothing III (upper graph) and from smoothing I (lower graph)

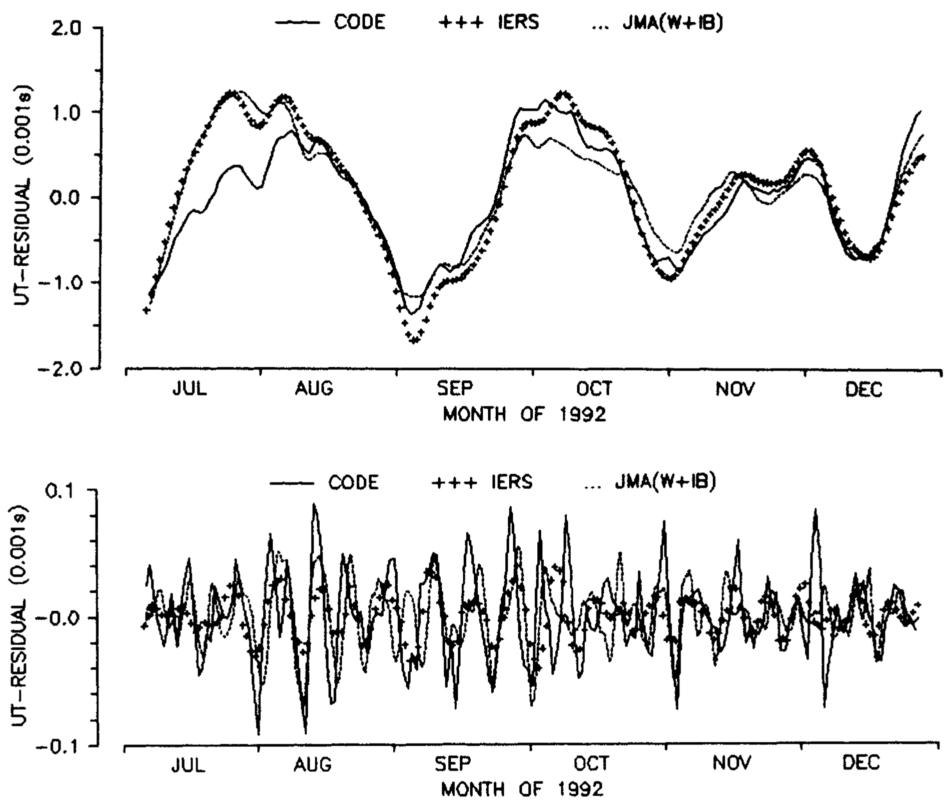

Fig.4 UT1R residuals from smoothing III (upper graph) and from smoothing I (lower graph)

DIFFERENCES OF EOP SERIES - UNCERTAINTIES AND CORRELATIONS

The residuals of GPS solutions, combined series and AAM series (with IB and without IB) representing the monthly, weekly and daily variations are compared pair by pair. Table 2 gives the estimates of rms differences after removing bias. As we are analyzing the residuals, bias of their differences is close to zero. For pairs of GPS series also the corresponding formal uncertainties based on information from processing centers are shown. Fig.5 is a plot of rms differences between GPS solutions. Displayed are also rms differences between JPL GPS series and IRES combined solution - two series with the best mutual agreement.

Table 3 summarizes correlation coefficients for pairs considered in Table 2. Correlation exceeding critical values at 0.01 significance level is found for each pair of geodetic series except the difference between SIO and CODE daily variations (0.05 level). Correlation coefficients between GPS series and between JPL and combined series are shown in Fig.6.

Table 2
Rms differences of various pole coordinates series (units 0.001"). Unc. means the formal uncertainty of GPS series differences.

Series	Filter	JPL	IERS	SIO	AAM (NIB)	AAM (IB)
CODE	III x	0.89	0.95	1.09	2.23	1.75
	y	1.00	0.85	0.98	2.14	1.53
	II x	0.70	0.80	0.95	1.03	1.11
	y	0.71	0.79	0.91	1.07	0.95
	I x	0.48	0.59	0.70	0.57	0.58
	y	0.51	0.56	0.66	0.61	0.58
	Unc.	0.20	-	0.23	-	-
AAM(IB)	III x	1.40	1.42	1.48		
	y	1.07	1.23	1.48		
	II x	0.67	0.80	0.75		
	y	0.63	0.53	0.74		
	I x	0.17	0.14	0.39		
	y	0.23	0.13	0.42		
	Unc.	-	-	-		
AAM(NIB)	III x	2.04	1.98	2.26		
	y	2.18	1.98	2.07		
	II x	0.71	0.75	0.82		
	y	0.74	0.72	0.89		
	I x	0.25	0.21	0.46		
	y	0.31	0.23	0.42		
	Unc.	-	-	-		
SIO	III x	0.89	0.77			
	y	0.87	0.71			
	II x	0.58	0.64			
	y	0.43	0.53			
	I x	0.35	0.42			
	y	0.31	0.38			
	Unc.	0.26	-			
IERS	III x	0.82				
	y	0.69				
	II x	0.48				
	y	0.39				
	I x	0.18				
	y	0.23				
	Unc.	-				

Table 3
Correlation coefficients for x and y pole coordinates
Crit. means the critical value for α=0.01.

Series	Filter	JPL	IERS	SIO	AAM (NIB)	AAM (IB)
CODE	III x	0.97	0.89	0.82	0.57	0.54
	y	0.81	0.86	0.84	0.48	0.37
	II x	0.78	0.74	0.55	0.54	0.38
	y	0.68	0.73	0.53	0.40	0.40
	I x	0.44	0.36	0.15	0.42	0.48
	y	0.37	0.30	0.20	0.16	0.18
	Crit.	0.22	0.18	0.21	0.22	0.22
AAM(IB)	III x	0.65	0.65	0.60		
	y	0.51	0.45	0.44		
	II x	0.43	0.51	0.60		
	y	0.45	0.60	0.22		
	I x	0.34	0.61	0.35		
	y	0.33	0.49	0.34		
	Crit.	0.22	0.18	0.21		
AAM(NIB)	III x	0.65	0.66	0.50		
	y	0.51	0.55	0.49		
	II x	0.57	0.65	0.55		
	y	0.61	0.63	0.47		
	I x	0.49	0.68	0.28		
	y	0.34	0.61	0.34		
	Crit.	0.22	0.18	0.21		
SIO	III x	0.91	0.91			
	y	0.89	0.91			
	II x	0.71	0.73			
	y	0.84	0.72			
	I x	0.49	0.31			
	y	0.64	0.39			
	Crit.	0.26	0.21			
IERS	III x	0.91				
	y	0.88				
	II x	0.85				
	y	0.83				
	I x	0.50				
	y	0.43				
	Crit.	0.18				

Standard deviations and correlations for pairs of UT1R series - GPS, combined, daily VLBI and AAM are given in Table 4 and Table 5. The statistics obtained for weekly variations and daily variations have similar value for all compared series. This proves that GPS observed variations are reliable for periods shorter than one month.

Table 4
Rms differences between GPS, daily VLBI, IERS combined and atmospheric UT series (units 0.001 ms)

Series	Filter	IERS	VLBI	AAM
CODE	III	0.507	0.527	0.522
	II	0.103	0.096	0.093
	I	0.034	0.048	0.037
AAM	III	0.229	0.298	
	II	0.108	0.093	
	I	0.021	0.041	
VLBI	III	0.261		
	II	0.093		
	I	0.036		

Table 5
Correlation coefficients between GPS, daily VLBI, IERS combined and atmospheric UT series.
Crit. means the critical value at significance level α=0.01.

Series	Filter	IERS	VLBI	AAM
CODE	III	0.77	0.71	0.71
	II	0.80	0.80	0.79
	I	0.39	0.17	0.37
	Crit.	0.18	0.24	0.18
AAM	III	0.96	0.91	
	II	0.78	0.80	
	I	0.50	0.14	
	Crit.	0.18	0.24	
VLBI	III	0.94		
	II	0.84		
	I	0.23		
	Crit.	0.24		

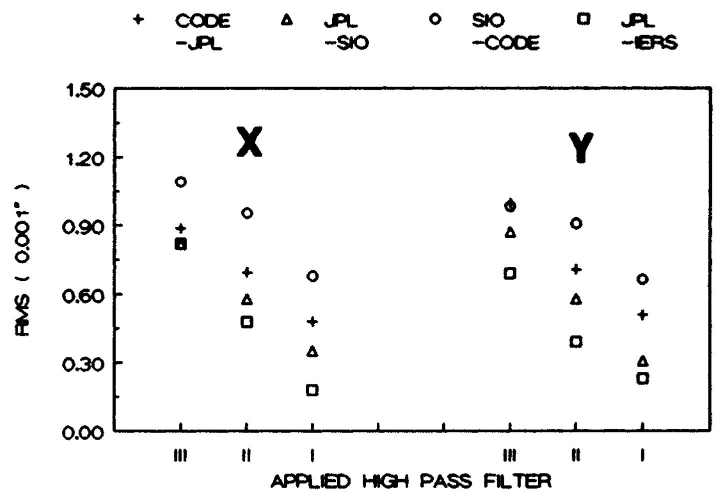

Fig.5 Rms differences of polar motion series

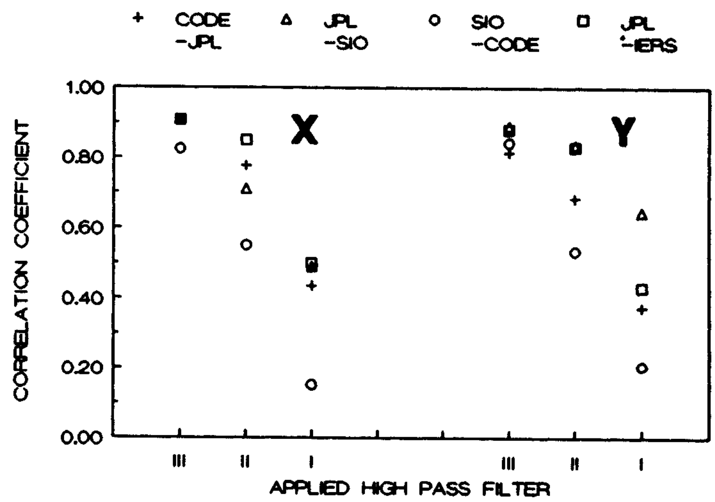

Fig.6 Correlation coefficients between polar motion series

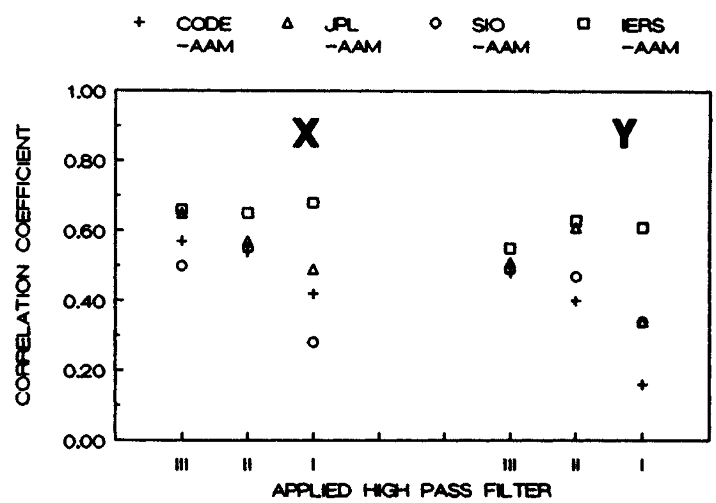

Fig.7 Correlation coefficients between geodetic and AAM polar motion

CONCLUSIONS

The short-term polar motion variations in range from days to months observed by GPS are at 0.5 - 5 mas level according to used high pass filtering and significantly exceed the formal uncertainties. Rms differences for pairs of geodetic series (GPS and combined) are bellow 1 mas and gradually decrease towards high frequencies. Correlations between geodetic series is also decreasing but remains significant for daily variations except the SIO-CODE pair. Significant correlation 0.4 - 0.6 results from comparison of GPS polar motion series with both IB and without IB approximation atmospheric models.

Monthly, weekly and daily non-tidal UT variations are well observed by GPS CODE series. The monthly GPS oscillations exhibit the most significant discrepancies with other geodetic series, especially in the beginning of IGS campaign. The atmospheric driving of short-term Earth's rotation is recognized by GPS at the time scales from days to months.

ACKNOWLEDGEMENT

Author thanks N. Essaifi from IERS/CB for providing the GPS EOP series and I. Naito and Y. Tamura from NAO Mizusawa for granting the atmospheric angular momentum data.

REFERENCES

[1] IERS,"1991 IERS Annual Report",Central Bureau of IERS, Observatoire de Paris, 1992

[2] Yoder,C.F.,Williams,J.G.,Parke,M.E.,"Tidal Variations of Earth Rotation", J.Geophys.Res.,86,881-891, 1981.

[3] Ozaki,T., Kuma,K., Kikuchi,N., Naito,I., "Effective Atmospheric Angular Momentum Functions Computed from the Japan Meteorological Agency Data", Priv. Comm., 1993.

[4] Gross R.S., Lindqwister U.,"Comparison of GIG'92 Polar Motion Results with Atmospheric Angular Momentum CHI Functions", JPL Geodesy and Geophysics Preprint No.222, 1992.

[5] Vondrak,J.,"A Contribution to the Problem of Smoothing Observational Data", Bull. Astron. Inst. Czechosl. 20, 349-355, 1969.

SHORT PERIODIC OSCILLATIONS IN GPS POLE COORDINATES DATA

W. KOSEK
Space Research Centre, PAS
ul. Bartycka 18a, 00–716 Warsaw
Poland

ABSTRACT. The 3.5 day oscillation has been found in GPS x, y pole coordinates data determined by different processing centers in July 1992 - March 1993 using the Band Pass Filter Spectral Analysis and the Ormsby band pass filter.

1. Introduction

Earth rotation parameters have recently been obtained from networks observing Global Positioning System (GPS) satellites (Herring et al., 1991; Lichten et al., 1992). Analyses of GPS data of pole positions indicate about 0.5 mas agreement with the VLBI estimates (Lindqwister et al., 1992). The GPS results are obtained usually from one day observations of 16-18 satellites in a network of different number of stations ranging from 10 to about 30. The analysis of 17-60 days common time intervals between the pairs of series of x, y pole coordinates during the SEARCH 92' Campaign found no significant correlation between them (IGS'92 Campaign third report, 1992).

2. Analysis of GPS pole coordinates data

The pole coordinates series from the following centers and data intervals have been used in order to analyze the short periodic oscillations from 2 to about 15 days in pole coordinates data:

BERNE (University of Berne (AIUB)) 48792.5-49042.5
EMR (Energy Mines and Resources, Canada) 48838.5-49038.5
ESOC (European Space Operations Center) 48794.5-49038.5
GFZ (GeoForschungsZentrum, Potsdam) 48795.0-48925.5
JPL (Jet Propulsion Laboratory, Pasadena) 48794.5-49024.5
SCRIPPS (Scripps Institute (UCSD)) 48780.5-49038.5
UTX (University of Texas at Austin) 48794.5-48870.5
COMBIN (U.S. Naval Observatory, Washington D.C.) 48781.0-49042.0

The sampling interval of all these data is equal to 1 day except the GFZ solution in which there is a 1.5 day gap in the middle of data and some gaps noticed in the UTX, EMR and ESOC solutions. All the data were interpolated at 1 day time intervals using the first order linear interpolation.

Next, long periodic and the Chandler and annual oscillations were removed by computation of the second difference by the following formula:

$$\Delta^2 x_{j,k} = x_{j+2,k} - 2x_{j+1,k} + x_{j,k}, \tag{1}$$

where $x_{j,k}$ are data points of kth solution interpolated at the moments of $t_m = 48792.5 + \Delta t(m-1)$, Δt is the sampling interval.

This second difference is the high pass filter enlarges amplitudes of high frequency oscillations ranging from $\frac{1}{2\pi\Delta t}$ to $\frac{1}{2\Delta t}$. The band pass filter spectral analysis (BPFSA) (Kosek, 1991) has been applied in order to compute spectrum estimations by the following formula:

$$\hat{S}(\lambda_o) = \frac{1}{N(k) - 2L + 1} \sum_{j=1}^{N(k)-2L+1} [\sum_{l=-L}^{L} \Delta^2 x_{j+l,k} h_l(\lambda_o)]^2 \tag{2}$$

where $\frac{\Delta t}{15days} < \lambda_o < \frac{\Delta t}{2days}$, $N(k)$ is the number of interpolated data of kth solution, L is the length of the Ormsby band pass filter with the impulse response given by the following formula:

$$h_l(\lambda_o) = \frac{2sin(\pi l\lambda)cos(2\pi\lambda_o)sin(2\pi\beta)}{\lambda(\pi l)^2} \tag{3}$$

where λ is the transition band, β is the half of the sum of the pass band and the transition band, $\lambda_o = \frac{\Delta t}{T_o}$ is the normalized frequency, for which the oscillation with period T_o is computed.

The spectra $\hat{S}(\lambda_o)$ have been computed assuming $\lambda = 0.03$, $\beta = 0.03$ and $L = 50$. In these spectra (Fig. 1) two main peaks correspond to about 2.4 and 3.5 days oscillations except the spectrum of the COMBIN solution where the power corresponds to the lower frequency oscillations. The COMBIN solution does not represent the solutions determined by different processing centers in the case of short periodic oscillations. The weighted mean which enables to transfer all frequency information to the output has been computed by the following formula:

$$\hat{x}_m = \frac{\sum_{k=1}^{M} x_{j,k} p_{j,k}}{\sum_{k=1}^{M} p_{j,k}} \quad for \quad j = 1, 2, ..., N(k) \tag{4}$$

where $M = 7$ is the number of solutions and the weight of such interpolated point is assumed:

$$p_{j,k} = \frac{t_{i+1,k} - t_{i,k}}{\hat{\sigma}^2_{x_{i,k}}(t_{i+1,k} - t_m) + \hat{\sigma}^2_{x_{i+1,k}}(t_m - t_{i,k})} \tag{5}$$

where $t_{i,k}$ is the MJD of data $x_{i,k}$.

Usually all these data are equidistant, so $t_m = t_{i,k}$ and the weight of the point is expressed by $p_{j,k} = 1/\hat{\sigma}^2_{x_{i,k}}$ where $\hat{\sigma}^2_{x_{i,k}}$ is the RMS of the ith point in the kth solution.

The spectrum of the second difference of such weighted data has the peaks corresponding to around 2.5 and 3.5-4.0 day oscillations and looks very similar to the spectra of solutions from different processing centers (Fig. 1).

3. Model data analysis

The spectra of x, y pole coordinate second differences computed by the BPFSA do not have the confidence intervals for their values and its difficult to say whether detected peaks are real or not. In order to check the reality of detected peaks in x, y pole coordinates the BPFSA spectra have been also computed for the model data of 260 data points sampled at 1 day intervals. This model consists of the Chandler oscillation with the amplitude of 200 mas, the annual oscillation with the amplitude of 100 mas and the white noise with standard deviation of 1 mas. The spectra computed for the second difference of such 4 different model data increase their power almost monotonically toward higher frequencies and show no significant power around 3.5 day oscillation (Fig. 2).

4. The 3.5 days oscillation determined by the Ormsby filter

Next, the Ormsby band pass filter has been applied in order to compute the 3.5 day oscillation in the second difference of pole coordinates. The parameters of the Ormsby band pass filter are the same as for the spectrum computation except the filter length, which was reduced to $L = 30$. The amplitude of the output was multiplied by the factor of $-(\frac{3.5days}{2\pi\Delta t})^2$ in order to convert it to the amplitude of data. In the case of x, y pole coordinates of BERNE. SCRIPPS, and JPL there is some agreement in phase and in some sense in the amplitude of 3.5 day oscillations (Fig. 3). This amplitude is variable and of the order of 0.3 mas.

5. Conclusions

The COMBIN solution computed from 7 GPS pole coordinates does not contain information about short periodic oscillations from 2 to about 15 days.

The Ormsby band pass filter spectra of second differences of GPS x, y pole coordinates have the common peaks corresponding to 3.5 and about 2.5 days oscillations. There is some phase and amplitude agreement of the 3.5 days oscillations in the case of BERNE, SCRIPPS and JPL solutions.

Acknowledgements. I thank very much Dr. D.D. McCarthy from the U.S. Naval Observatory for the GPS pole coordinates data and Dr. B.E. Schutz, R. Eanes and M. Watkins for comments that helped me to fulfill this work during my stay in the CSR in 1993.

References

Burg J.P. (1967). Maximum Entropy Spectral Analysis, 37th Ann. Int. Meet. Society of Exploration Geoph., Oklahoma City, October 31, 1967.

IGS'92 Campaign (1992). Comparison of GPS, SLR and VLBI Earth Orientation Determinations (third report). IERS, Bureau Central de L'IERS Observatoire de Paris.

Kosek W. (1991). On high frequency spectral analysis of very noisy stochastic processes and its application to the ERP series determined by VLBI and SLR. U.S. Naval Observatory Circular No 177, Washington D.C. 20392-5100, Feb., 15.

Lichten S.M., Marcus S.L. and Dickey J.O. (1992). Sub-Daily Resolution of Earth Rotation variations with Global Positioning System Measurements, Geoph. Res. Letters, 19, 537-540, 1992.

Lindqwister U.J., Freedman A.P., Blewitt G. (1992). Daily Estimates of Earth's Pole Positions with Global Positioning System., Geoph. Res. Letters., 19, 845-848, 1992.

Ormsby J.F.A. (1961). Design of Numerical Filter with Application of Missile Data Processing., J. Assoc. Comput. Mach. 8, pp 440-466.

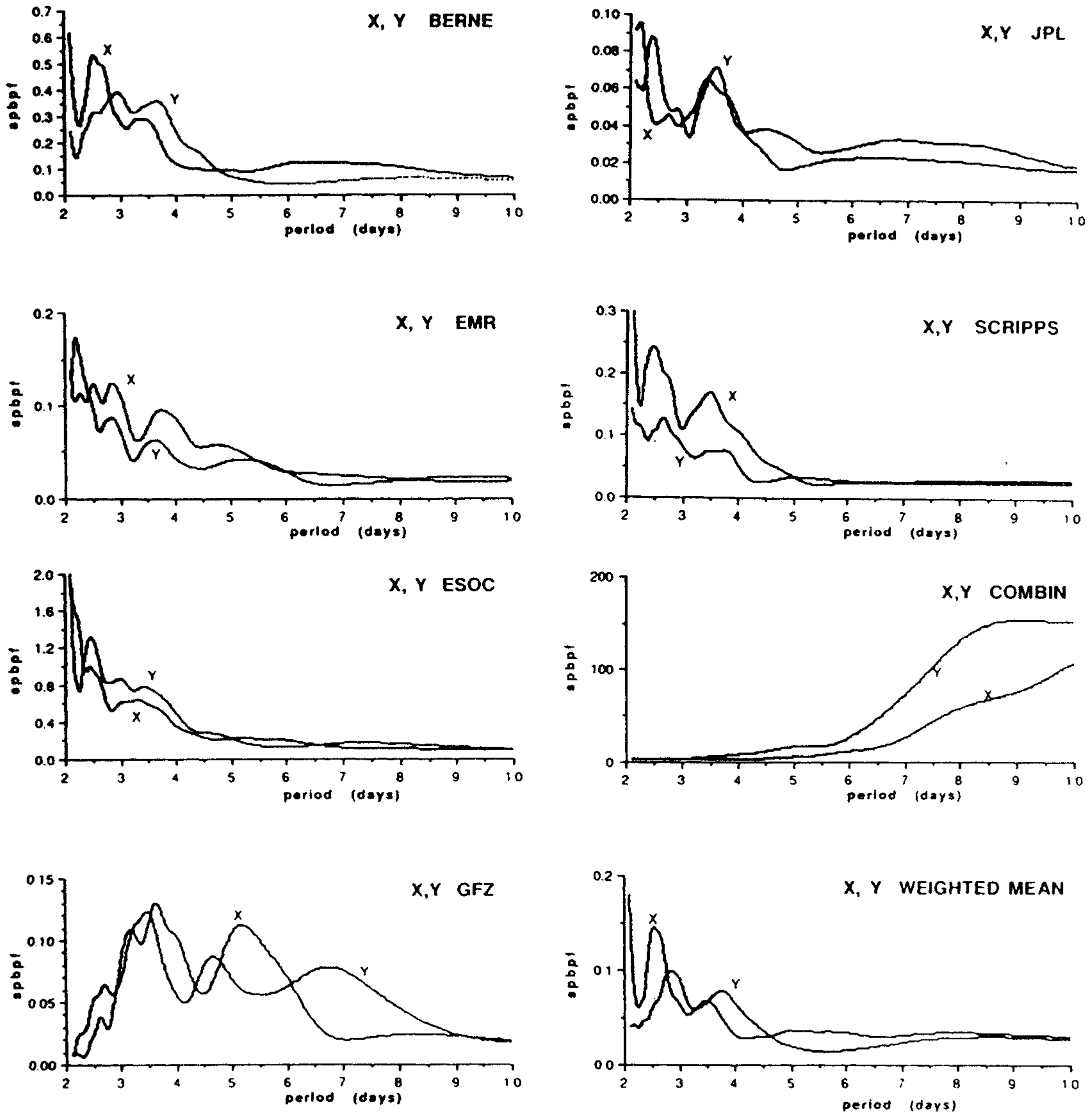

Fig. 1. The BPFSA spectra of the second difference of pole coordinates determined by different processing centers.

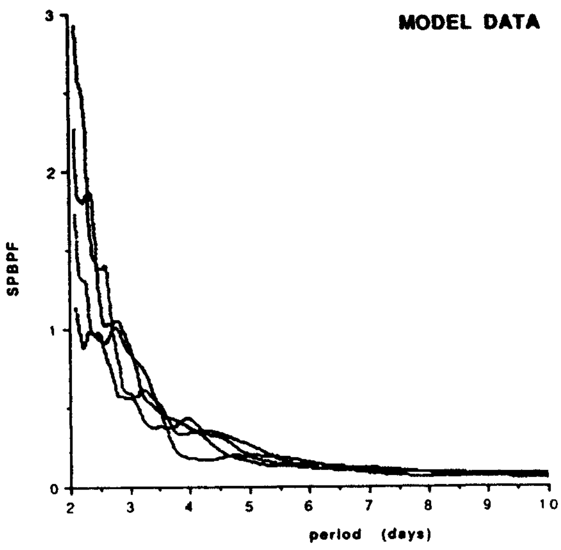

Fig. 2. The BPFSA spectra of the second difference of 4 model data.

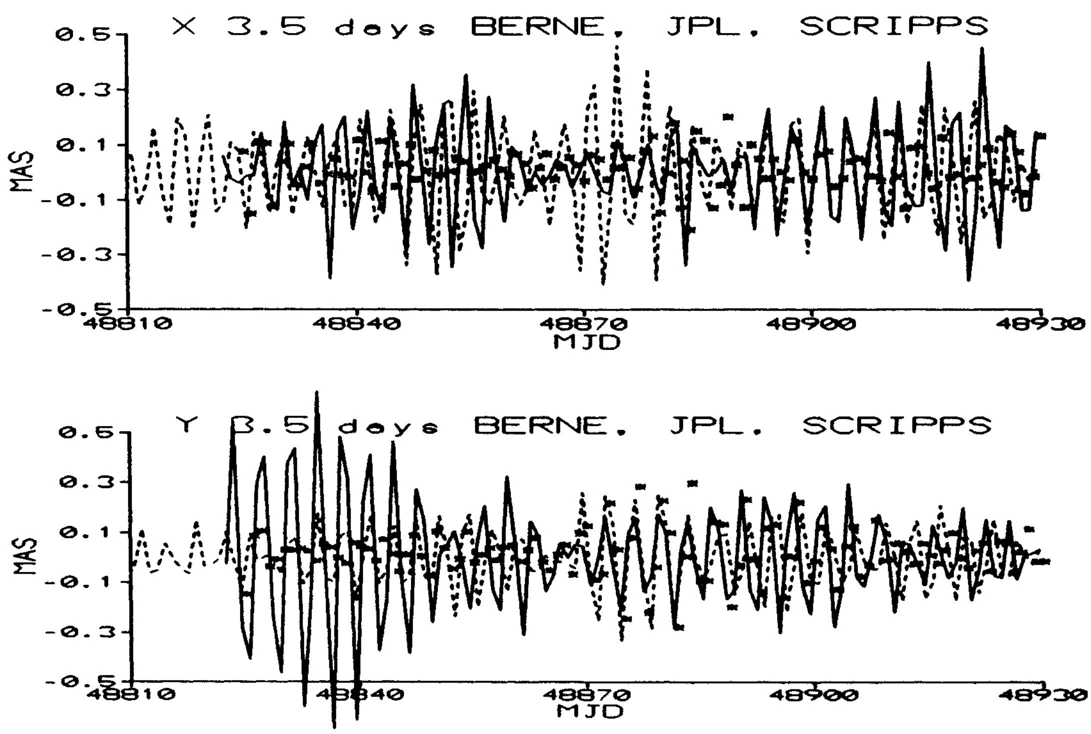

Fig. 3. 3.5 day oscillation computed by the Ormsby band pass filter in x,y pole coordinates determined by BERNE (thin line), JPL (stars), SCRIPPS (dotted line).

COMPARISON OF WET DELAY ESTIMATES USING VLBI, GPS, AND WVR DATA AT THE ONSALA SPACE OBSERVATORY DURING SEARCH'92

G. Elgered, J. M. Johansson
Onsala Space Observatory, Chalmers University of Technology
S–439 92 Onsala
Sweden

J. L. Davis
Harvard–Smithsonian Center for Astrophysics
60 Garden St., CAMBRIDGE, MA 02138
USA

ABSTRACT. Unmodeled variations in the wet propagation delay are a major source of error in space geodetic techniques using radio signals, such as VLBI and GPS. The most common method to deal with this error is to estimate the equivalent zenith wet delay at each site. Wet delays estimated using VLBI and GPS data are compared with microwave radiometer measurements.

1. Introduction

It is well known that the varying amount of atmospheric water vapor affects the propagation time of a radio signal. The common method to deal with this excess propagation time in radio based space geodetic techniques is to estimate an atmospheric correction using the geodetic data themselves. This correction may be modelled as a constant, a piece-wise linear function, or a stochastic process. In this study we compare estimates of the wet propagation delay using two space geodetic techniques, Very-Long-Baseline Interferometry (VLBI) and the Global Positioning System (GPS) with estimates from a ground-based microwave radiometer. The model used in both the VLBI and the GPS analysis is a Markov process or more specifically a random walk process.

The variance between values separated by the time Δt for a random walk process scales linearly with the separation

$$< (x(t+\Delta t) - x(t))^2 >= \sigma^2 \, \Delta t \qquad (1)$$

In addition to study the influence of the wet delay on the accuracy of VLBI and GPS another goal of this work is to evaluate the use of GPS networks for meteorological measurements (see, *e.g.*, Bevis et al. (1992)).

2. Instrumentation and Estimation Techniques

The maximum distance between the 20 meter radio telescope used for VLBI observations, the GPS antenna and the Water Vapor Radiometer (WVR) is approximately 80 m. The intersection of azimuth and elevation axises of the VLBI antenna is 22 m above the mean sea level whereas both the GPS and WVR antenna heights above sea level are 9 m. This means that for a standard atmosphere with a scale height equal to 2 km the VLBI antenna senses a wet delay which is 0.6% less than the other two methods. This effect is of the order of 1 mm and will be ignored in the following.

Three contiguous 24 hour long VLBI experiments were carried out during July 1992. The two first were dedicated mobile experiments and the third was IRIS-A 751. All of them included the mobile VLBI antenna (MV-2) at Høfn, Iceland. Because of the lower sensitivity of the mobile VLBI antenna typically 180 observations were carried out during one 24 hour experiment. For example, the R&D experiments during 1993, using larger antennas, typically include 300 observations at each site.

The GPS receiver, a Rouge SNR-800 with a Dorne-Margolin antenna operated continuously without any problems during this time period.

The WVR, measuring the atmospheric emission at 21.0 and 31.4 GHz was operated in a "sky mapping mode" with a cycle of approximately 8 minutes rather than pointing at each VLBI source. Approximately 60 observations spread over the sky down to an elevation angle of 23° was acquired during one such cycle.

The VLBI estimates use observations down to elevation angles of approximately 7°. The hydrostatic mapping function is used to calculate the actual hydrostatic delay from the equivalent zenith value based on ground pressure observations (Davis et al. 1985). The wet delay is estimated using a special wet delay mapping function (Chao 1972). The VLBI data analysis is carried out with the SOLVK software (Herring et al. 1990). The value of the random walk variance, σ^2 in (1), is estimated for each site using the delay rate residuals. For the three experiments the estimated values of σ^2 were 0.19, 0.90, and 0.46 ps^2/s, respectively.

The GPS estimates use observations down to an elevation angle of 15°. One mapping function (Lanyi 1984) is used to estimate the total propagation delay in the GIPSY software (Lichten and Border 1987). The standard value used for the data in this study was 0.32 ps^2/s. The wet delay is, thereafter, calculated by subtracting the zenith value of the hydrostatic delay based on the ground pressure observations. In this presentation a mean ground pressure has been used for each day but this will be improved in the near future.

The microwave radiometer data are presented as equivalent zenith values of actual observations at different elevation angles using the simple cosecant law. In this data set the radiometer was scanning the entire sky but always above an elevation angle of 23°. Otherwise the typical observation strategy using the WVR is to observe in the same direction as the VLBI antenna and perform so called tip-curves during the time between the VLBI observations.

3. Results

Below we present the estimated wet delays using the three different methods. Figure 1 shows the results when the GPS data were processed in 24 hour long daily data sets independently. It should be noted that when we processed the first two days of GPS data, the large increase in the wet delay around midnight between July 25–26 is in better agreement with the WVR and the GPS data. The VLBI processing has been made independently for each experiment.

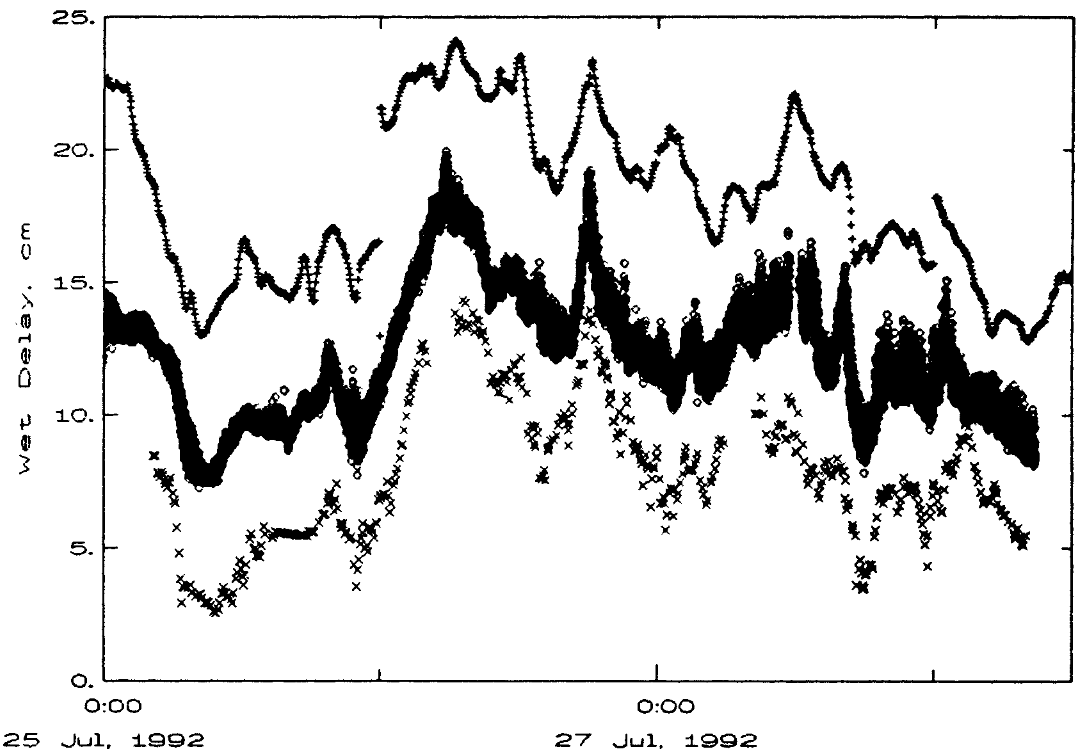

Figure 1. Comparison between estimated equivalent zenith wet delays using GPS, VLBI and microwave radiometer data. In order to make it easier to compare the results biases of +5 cm and -5 cm have been added to the GPS (upper curve) and VLBI (lower curve) estimates, respectively. The microwave radiometer data (middle curve) have been acquired by scanning the instrument in azimuth and elevation in a cycle repeated every 12 minutes.

4. Discussion

Slowly varying differences at the centimeter level exist between all data sets. The typical mean biases calculated for one day is about 1 cm. This is true also when the imperfect correction of the hydrostatic delay in the GPS data sets is taken into account.

The WVR data are less accurate when there are large amounts of liquid water in the atmosphere. An advantage is, however, that the liquid water content can be estimated simultaneously with the wet delay using the WVR data. In this presentation we have discarded all data for which the estimated integrated liquid water content is larger than 0.7 mm. In the evening of July 26 the rapid increase suggested by the WVR data is supported by the VLBI data. (The liquid water content at the peak is 0.7 mm.) On the other hand events with a liquid water content of 0.7 mm have been seen in other data sets where the WVR data seem to overestimate the wet delay.

5. Conclusions and Future Work

Variations in the wet propagation delay are in general "detected" by all three methods.

This type of comparison has proven valuable for detecting errors (such as ignored clock-breaks) in the VLBI and the GPS data analysis.

As more data are being analyzed the goal is to search for systematic differences in the wet delay estimates.

References

Bevis, M., S. Businger, T.A. Herring, C. Rocken, R.A. Anthes, and R.H. Ware (1992), GPS Meteorology: Remote Sensing of Atmospheric Water Vapor Using the Global Positioning System, *J. Geophys. Res.*, **97**, pp. 15787–15801.

Chao, C.C., A model for tropospheric calibration from daily surface and radiosonde balloon measurements (1972), *Tech. Mem. 391-350*, Jet Propulsion Lab., Pasadena, California.

Davis, J.L., T.A. Herring, I.I. Shapiro, A.E.E. Rogers, and G. Elgered, Geodesy by Radio Interferometry: Effects of Atmospheric Modeling Errors on Estimates of Baseline Length (1985), *Radio Sci.*, **20**, pp. 1593–1607.

Herring, T.A., J.L. Davis, and I.I. Shapiro, Geodesy by radio interferometry: The application of Kalman filtering to the analysis of very long baseline interferometry data (1990), *J. Geophys. Res.*, **95**, pp. 12,561–12,581.

Lanyi, G., Tropospheric delay effects in radio interferometry (1984), *TDA progress report 42–78*, Jet Propulsion Laboratory, Pasadena, California.

Lichten, S.M., and J.S. Border, Strategies for high-precision Global Positioning System orbit determination (1987), *J. Geophys. Res.*, **92**, pp. 12751–12762.

Reproduit par INSTAPRINT S.A. – 1-2-3, levée de la Loire – LA RICHE – B.P. 5927 – 37059 TOURS Cedex – Tél. 47 38 16 04

Dépôt légal 3ème trimestre 1994